ARTICLE IN PRESS

Journal of Computational Physics xxx (2010) xxx–xxx

Contents lists available at ScienceDirect

Journal of Computational Physics

journal homepage: www.elsevier.com/locate/jcp

Modeling and computation of two phase geometric biomembranes using surface finite elements

Charles M. Elliott, Björn Stinner *

Mathematics Institute, Zeeman Building, University of Warwick, Coventry CV4 7AL, United Kingdom

ARTICLE INFO

Article history:
Received 12 September 2009
Received in revised form 8 March 2010
Accepted 17 May 2010
Available online xxxx

Keywords:
Lipid bilayer
Multi-component membrane
Phase field method
Relaxation dynamics
Numerical simulation
Surface finite element method

ABSTRACT

Biomembranes consisting of multiple lipids may involve phase separation phenomena leading to coexisting domains of different lipid compositions. The modeling of such biomembranes involves an elastic or bending energy together with a line energy associated with the phase interfaces. This leads to a free boundary problem for the phase interface on the unknown equilibrium surface which minimizes an energy functional subject to volume and area constraints. In this paper we propose a new computational tool for computing equilibria based on an L^2 relaxation flow for the total energy in which the line energy is approximated by a surface Ginzburg–Landau phase field functional. The relaxation dynamics couple a nonlinear fourth order geometric evolution equation of Willmore flow type for the membrane with a surface Allen–Cahn equation describing the lateral decomposition. A novel system is derived involving second order elliptic operators where the field variables are the positions of material points of the surface, the mean curvature vector and the surface phase field function. The resulting variational formulation uses H^1 spaces, and we employ triangulated surfaces and H^1 conforming quadratic surface finite elements for approximating solutions. Together with a semi-implicit time discretization of the evolution equations an iterative scheme is obtained essentially requiring linear solvers only. Numerical experiments are presented which exhibit convergence and the power of this new method for two component geometric biomembranes by computing equilibria such as dumbbells, discocytes and starfishes with lateral phase separation.

1. Introduction

Lipid bilayer membranes, in the following called biomembranes, are ubiquitous in living organisms as they form the boundaries of cells and cell organelles, but also are of interest in the pharmaceutical industry which intends to use vesicles for drug transport. The mechanics of the biomembranes are important in understanding cell shapes and their transitions from one configuration to another [36]. Established models of lipid bilayer membranes treat them as deformable inextensible fluid surfaces of infinitesimal thickness unable to sustain shear stress. This leads to postulating bending energy functionals with the membrane strain energy depending on the curvature of the surface. Biomembranes exhibit an interesting variety of shape transitions, i.e. the formation of buds, pearling and vesicle fission. Such phenomena have recently been observed in multi-component giant unilamellar vesicles (GUVs) involving a separation into two phases [3,4].

In this paper we present a method for computing equilibrium shapes of vesicles formed by geometric biomembranes that involve a lateral separation into two phases. We define a relaxation dynamics by means of a gradient flow of the membrane energy, derive a variational formulation using a surface calculus summarized in the Appendix, and we employ H^1 conforming

* Corresponding author. Tel.: +44 (0)24 7615 0261; fax: +44 (0)24 7652 4182.
E-mail address: bjorn.stinner@warwick.ac.uk (B. Stinner).

0021-9991/$ - see front matter © 2010 Elsevier Inc. All rights reserved.
doi:10.1016/j.jcp.2010.05.014

isoparametric quadratic surface finite elements in order to approximate solutions to the evolution equations. We consider vesicles governed by energy

$$\mathcal{F}(\Gamma) := \mathcal{F}_W(\Gamma) + \mathcal{F}_\gamma(\Gamma) + \mathcal{F}_M(\Gamma) := \int_\Gamma \frac{k_H}{2}|H|^2 + \int_\gamma \bar{\sigma} + \frac{k_H\alpha}{8}(m-m_0)^2 \tag{1.1}$$

and use the phase field approximationc

$$\mathcal{F}(\Gamma, c) := \mathcal{F}_W(\Gamma) + \mathcal{F}_{GL}(\Gamma, c) + \mathcal{F}_M(\Gamma) := \int_\Gamma \frac{k_H}{2}|H|^2 + \int_\Gamma \sigma\left(\frac{\varepsilon}{2}|\nabla_\Gamma c|^2 + \frac{1}{\varepsilon}W(c)\right) + \frac{k_H\alpha}{8}(m-m_0)^2 \tag{1.2}$$

The membrane is modeled as a closed hypersurface Γ in $\mathbb{R}^3$. Its mean curvature is denoted by H (sum of the principal curvatures, hence twice the mean curvature in the notation of other articles), and the field c is an order parameter (or phase field) defined on Γ that serves to distinguish the two possible intra-membrane phases. The equilibrium equations for critical points of the energy as well as the parabolic evolution equations of the relaxation flow are a highly nonlinear fourth order partial differential equation for the surface coupled to an Allen–Cahn partial differential equation on the surface for the phase field:

$$\begin{aligned} v_{\boldsymbol{\nu}} &= k_H\left(\Delta_\Gamma H + |\nabla_\Gamma \boldsymbol{\nu}|^2 H - \frac{1}{2}H^2\right) + \sigma\varepsilon\nabla_\Gamma c \otimes \nabla_\Gamma c : \nabla_\Gamma \boldsymbol{\nu} - \left(\frac{\sigma\varepsilon}{2}|\nabla_\Gamma c|^2 + \frac{\sigma}{\varepsilon}W(c)\right)H \\ &\quad + \frac{k_H\alpha}{4\overline{R}}(m-m_0)(|\nabla_\Gamma \boldsymbol{\nu}|^2 - H^2) - \lambda_V - (\lambda_A + \lambda_c h(c))H, \end{aligned}$$

$$\varepsilon\omega\partial_t^\bullet c = \varepsilon\sigma\Delta_\Gamma c - \frac{\sigma}{\varepsilon}W'(c) - \lambda_c h'(c)$$

where $v_{\boldsymbol{\nu}}$ is the (scalar) normal velocity, $\boldsymbol{\nu}$ is the unit normal, $\partial_t^\bullet$ the material derivative, λ_V,λ_A, and λ_c are Lagrange multipliers associated with constraints on enclosed volume and the areas of the two phases, and $\omega > 0$ is a kinetic coefficient. In general these equations are impossible to solve analytically but some insight can be gained in the case of axisymmetric geometries which lead to ordinary differential equations, see [31,32]. However in order to tackle non axisymmetric configurations and to consider further generalizations of the model it is necessary develop numerical discretizations of the general problem and this is the subject of this paper.

Let us first discuss the energy contributions and constraints:

- *Bending energy and line energy*
  A classical model for the elastic bending energy of a single phase membrane is the Canham–Helfrich–Evans energy functional [11,23,29] which in its simplest form reads

$$\mathcal{F}_{CEH}(\Gamma) := \mathcal{F}_W(\Gamma) + \mathcal{F}_K(\Gamma) := \int_\Gamma \frac{k_H}{2}H^2 + \int_\Gamma k_G K. \tag{1.3}$$

  Here K is the Gaussian curvature. The positive real numbers k_H (bending rigidity) and k_G (Gaussian bending rigidity) are material dependent elasticity parameters. For $k_H = 1, \mathcal{F}_W$ is known in differential geometry as the Willmore energy [40]. For simplicity we assume that the bending rigidities are the same in the two phases. By the Gauss–Bonnet theorem the last term is a topological invariant. Since we will confine our study to simply closed vesicles we will neglect this energy contribution.
  Line tension is also observed at the phase interface leading to the following energy functional for a two component membrane [31,32]:

$$\sum_{i=1}^{2}\mathcal{F}_W(\Gamma_i) + \mathcal{F}_\gamma(\Gamma) = \sum_{i=1}^{2}\left(\int_{\Gamma_i}\frac{k_H}{2}H^2\right) + \int_\gamma \bar{\sigma} \tag{1.4}$$

  where the membrane is composed of two smooth surfaces Γ_i with a common boundary γ. Then $\bar{\sigma}$ denotes the energy density of the excess free energy of the phase transition located on γ. It is commonly assumed that the lipid bilayer structure of the membrane remains intact across the phase interface so that the whole surface $\Gamma = \Gamma_1 \cup \gamma \cup \Gamma_2$ is at least of the class C^1.
- *Bilayer area difference*
  If the lipid molecules are strongly suppressed from changing sides of the bilayer then also the density difference between the bilayers is constant in equilibrium. This can be formulated as a condition on $M := \int_\Gamma H$. A common approach is not to formulate this as a hard constraint but as a soft one in the form of a penalty term by adding an energy of the form

$$\mathcal{F}_M(\Gamma) := \frac{k_H\alpha}{8}(m-m_0)^2, \quad m := \frac{M}{\overline{R}} = \frac{1}{\overline{R}}\int_\Gamma H \tag{1.5}$$

  to the membrane energy where m_0 is a given value and $\overline{R}$ a characteristic length scale (in fact $\overline{R} = \sqrt{|\Gamma|/4\pi}$ is the radius of a sphere with the same surface area as Γ), and α is a positive number. The factor αk_H sometimes is called the non-local bending rigidity and the model with the thus augmented energy is called area-difference-elasticity model (we refer to [36] Section 2.5.6 for a classification of commonly used models). Typically $\alpha \approx 1$, yet we treat this dimensionless

Please cite this article in press as: C.M. Elliott, B. Stinner, Modeling and computation of two phase geometric biomembranes using surface finite elements, J. Comput. Phys. (2010), doi:10.1016/j.jcp.2010.05.014

parameter rather as an independent parameter and in some simulations set it to zero, i.e. allowing the membrane to instantaneously exchange sufficient material between the two bilayers so that there is no lipid density difference.

- *Phase field line energy*
  As previously proposed in [1,37,39,33] we replace (or approximate) the line energy $\int_\Gamma \bar{\sigma}$ by a Ginzburg–Landau free energy of the form

$$\mathcal{F}_{GL}(\Gamma, c) := \int_\Gamma \sigma\left(\frac{\varepsilon}{2}|\nabla_\Gamma c|^2 + \frac{1}{\varepsilon}W(c)\right) \tag{1.6}$$

  where c is a phase field function (order parameter) to distinguish the two phases, ∇_Γ stands for the surface gradient, W is a double-well potential and ε a small length scale. The coefficient σ is proportional to the line energy density $\bar{\sigma}$ with a coefficient that depends on W. This double-well potential has two minima in the points $c = \pm 1$ so that $c \approx 1$ and $c \approx -1$ in the two phases, whilst the phase interface γ is replaced by a thin layer of a thickness scaling with ε across which c changes its value smoothly but quickly. For definiteness we take

$$W(c) = \frac{1}{2}(1 - c^2)^2$$

  which is the classical quartic double-well potential. The relation between line energy density and the coefficient in the Ginzburg–Landau energy is then given by, [22],

$$\bar{\sigma} = \frac{4}{3}\sigma \tag{1.7}$$

- *Area and volume constraints*
  Contributions to the elastic energy by expansion or contraction (changing the density of the lipids in the layers) but also by osmotic pressure may be several orders of magnitude larger than the energy contribution by bending, and such contributions can be modeled with effective constraints on the surface areas of the two phases and the volume of the enclosed domain (we refer to [36], Sec.2.4.4 for the physically relevant regime). Within the phase field methodology, the constraints on the areas of the two phases naturally are replaced by a constraint on the total surface area $|\Gamma|$ and on an integral involving the order parameter which in the simplest case reads $\int_\Gamma c$.

Minima of the Willmore bending energy $\mathcal{F}_W$ with constant $k_H = 1$ are called Willmore surfaces [40,18]. Several computational methods based on the use of surface finite elements on triangulated surfaces have been proposed to approximate the L^2 gradient flow of curvature dependent bending energies with and without area and volume constraints [34,18,2,9]. Other previous computational work include approaches on minimizing discrete versions of the membrane energy as in [30,8], the shape parameterization method in [7], the phase field approach [5,**?**,**?**,16], and a finite element method with C^1 elements [24,33]. We refer to [13] for a survey of numerical methods for geometric evolution equations. The novelty of our approach is the use of the phase field method on a moving hypersurface to deal with the line energy. We expect the mathematical and computational methodologies developed in this paper to be useful in developing methods for other models involving higher order surface energies and surface partial differential equations. Note that a fully three space dimensional phase field model can be employed as in [5,6,15,16]. However this is much more computationally demanding, requiring the solution of a fourth order PDE in three space dimensions in order to approximate the membrane surface. Grid adaptivity is mandatory, and there is the need for a careful investigation of topics such as the relation between the phase field parameters used for capturing the surface and the interface on the surface.

We observe the following about our method and the contributions of this paper:

- *Avoidance of parameterizations:* Our approach is intrinsic and does not require explicit formulae for parameterizations. It relies on the well known formula

$$-\Delta_\Gamma \boldsymbol{x} = H\boldsymbol{\nu} \tag{1.8}$$

  where Δ_Γ is the Laplace–Beltrami operator, $\boldsymbol{\nu}$ the unit normal to the surface, and $\boldsymbol{x}$:$\Gamma \to \Gamma$ the identity map.
- *Phase field approximation of line energy:* Using a phase field approximation of the line energy results in the motion of diffuse interfaces during the relaxation dynamics governed by an Allen–Cahn equation on the moving membrane surface. To solve such a problem on a triangulated surface we employ the computational methods developed in [19,20].
- *Variational formulation:* We derive a new variational formulation and gradient flow dynamics for the surface energy (1.2) and end up with a geometric evolution equation for the membrane surface coupled to partial differential equation on the moving surface describing the phase separation similar to that of [21] where a curvature flow with forcing term for a surface is coupled to a surface Cahn–Hilliard equation.
- *Mixed method and avoidance of C^1 elements:* The second order operator splitting of the fourth order partial differential equations for the membrane motion may be viewed as a mixed formulation. It allows the use of H^1 conforming and C^0 finite elements, and we can avoid C^1 finite elements as employed in [33].
- *Quadratic finite elements:* Although linear isoparametric surface finite elements would be sufficient we have used quadratic surface elements since approximating curvature and related geometric quantities is possible in better spaces,

Please cite this article in press as: C.M. Elliott, B. Stinner, Modeling and computation of two phase geometric biomembranes using surface finite elements, J. Comput. Phys. (2010), doi:10.1016/j.jcp.2010.05.014

[27,28,14]. Approximating a smooth surface by parametric quadratic finite elements based on a polyhedral surface (1.8) gives an approximation in L^2 of the mean curvature [28]. It is also our experience that the meshes associated with the quadratic finite elements maintained good quality during the evolution. We will introduce a mesh quality measure and report on it in the last section.

- *Iteration by semi-implicit time stepping:* Local minimizers of the energy are found by relaxing appropriate initial shapes to energetically favorable states. The governing equations consist of parabolic equations of second order for the phase separation and of fourth order for the membrane evolution where the latter one is split into two second order equations. In the full discretization the terms to highest order are taken implicitly in time whereas lower order terms may be taken explicitly in time so that the new iterates for the surface position $\boldsymbol{x}$, the mean curvature vector $\boldsymbol{H} = H\boldsymbol{\nu}$, and the order parameter c are computed in each relaxation step as the solution to linear systems. The method combines techniques of [18,19].
- *Hard constraints and Newton iteration:* The constraints on area, enclosed volume, and the order parameter integral are effectively ensured by performing Newton iterations at every relaxation step.
- *Convergence:* We document numerical experiments which indicate convergence of the numerical scheme with respect to the mesh size and the phase field interfacial thickness ε.
- *Quantitative results:* We compare the energies of relaxed axisymmetric membrane shapes with data from [32]. But the proposed method can also be used to explore the phase diagram of non-axisymmetric two-phase membranes. In this context we report on some simulations with discocytes involving a lateral phase-separation.
- *Software:* For the implementation the finite-element software ALBERTA [35] has been employed as well as the software UMFPACK [12] which is a direct solver for linear systems with sparse matrices.

The paper is organized as follows. In the next Section we present the equilibrium equations satisfied by critical points of the energy functional (1.4) including the constraints and their approximation by the diffuse interface model based on (1.2). Further, we formulate a relaxation dynamics via a gradient flow. In the Section after the surface finite elements are introduced and the governing equations are discretized. We also present the solution algorithm for the emerging discrete problem. Finally, in Section four we describe the results of significant numerical experiments that demonstrate the effectivity of the proposed method. In the Appendix we fix some notation and introduce concepts from differential geometry appropriate for our needs.

2. Mathematical models for two phase biomembranes

2.1. Phase-field surfaces and constraints

We now consider the phase field model with the line energy $\mathcal{F}_{GL}$ and define the objects on which we will set up the relaxation dynamics.

Definition 2.1 (*Admissible phase field surface*). An *admissible phase field surface* (Γ, c) for the membrane energy (1.2) is the smooth boundary Γ of a bounded, simply connected open domain $\Omega \subset \mathbb{R}^3$ such that Γ is diffeomorphic to the sphere together with a smooth field $c : \Gamma \to \mathbb{R}$ which is called an *order parameter* or *phase field variable*.

Most of the formulae presented in this section are valid for more general topologies of Γ which also are of practical importance (see [36, Figs. 4 and 5]). Yet we later on report only on simulation results for spherical membranes which is why restrict the analysis to this case.

As specified in the introduction we are interested in critical points (Γ, c) of $\mathcal{F}(\cdot,\cdot)$ defined by (1.2) subject to side conditions concerning the areas of the two phases and the volume of the enclosed domain. Let us denote the target value for the enclosed volume $|\Omega|$ by V and the target values for the areas of the two membrane domains $|\Gamma_i|$ by A_i, $i = 1, 2$. The fact that the sphere minimizes the area enclosing a given volume leads to the natural requirement on the data $\{V, A_1, A_2\}$ that

$$|\Gamma| = A_1 + A_2 \geqslant 4\pi(3V/4\pi)^{2/3} \tag{2.1}$$

where the right hand side is the area of the sphere enclosing the volume V.

To take the area constraints into account in the phase field model we consider the function

$$h(c) = \begin{cases} 1 & \text{if } 1 \leqslant c, \\ \frac{1}{2}c(3 - c^2) & \text{if } -1 < c < 1, \\ -1 & \text{if } c \leqslant -1 \end{cases}$$

and impose a constraint on $\int_\Gamma h(c)$ and on $|\Gamma|$. In fact, in the limit as $\varepsilon \to 0$ one expects that $\int_\Gamma h(c) \to |\Gamma_1| - |\Gamma_2|$. Since we want to preserve the areas of Γ_1 and Γ_2 in this limit, in the phase field approximation we preserve $\int_\Gamma h(c)$ and $|\Gamma| = |\Gamma_1| + |\Gamma_2|$ instead. We remark that this approach has been successfully applied previously in the context of Allen–Cahn systems on flat domains, cf. [25]. Denoting by $A_i > 0$ the prescribed surface areas of Γ_i, $i = 1, 2$ the constraint on the total area and on the phase area difference read

Please cite this article in press as: C.M. Elliott, B. Stinner, Modeling and computation of two phase geometric biomembranes using surface finite elements, J. Comput. Phys. (2010), doi:10.1016/j.jcp.2010.05.014

$$\mathcal{C}_A(\Gamma, c) = 0, \tag{2.2}$$
$$\mathcal{C}_c(\Gamma, c) = 0 \tag{2.3}$$

in terms of the functionals

$$\mathcal{C}_A(\Gamma) := |\Gamma| - (A_1 + A_2), \quad \mathcal{C}_c(\Gamma, c) := \int_\Gamma h(c) - (A_1 - A_2).$$

The constraint $\mathcal{C}_c$ will be called *mass constraint* in the following with the notion behind that $\int_\Gamma h(c)$ could correspond to some kind of mass.

Let $V > 0$ be the prescribed enclosed volume. Defining the functional

$$\mathcal{C}_V(\Gamma) := |\Omega| - V = \frac{1}{3}\int_\Gamma \boldsymbol{x}\cdot\boldsymbol{\nu} - V$$

the volume constraint reads

$$\mathcal{C}_V(\Gamma) = 0 \tag{2.4}$$

2.2. Variations of surface functionals

In this subsection we consider smooth hypersurfaces Γ which are the boundary of a simply connected open set $\Omega \subset \mathbb{R}^3$ and topologically are spheres. Given a smooth field $\boldsymbol{w} : \Gamma \to \mathbb{R}^3$ there is a τ_0 such that the sets

$$\Gamma(\tau) := \{\boldsymbol{x}(\tau) := \boldsymbol{x} + \tau \boldsymbol{w}(\boldsymbol{x}), \boldsymbol{x} \in \Gamma\}$$

have the same properties as Γ for all $\tau \in (-\tau_0, \tau_0)$.

Definition 2.2 (*Variation of surface functionals*). Let $\mathcal{E} = \mathcal{E}(\Gamma)$ be a surface functional and $\boldsymbol{w} : \Gamma \to \mathbb{R}^3$ be a deformation field. The variation of $\mathcal{E}$ in Γ in direction w is defined by

$$\langle D\mathcal{E}(\Gamma), \boldsymbol{w}\rangle := \frac{d}{d\tau}\mathcal{E}(\Gamma(\tau))\Big|_{\tau=0}$$

Before we consider the variations of the individual functionals appearing in the membrane energy and constraints, we state a helpful result which dates back to an idea of [18]. The variational curvature identity (A.3) which is the weak formulation of (1.8) holds true on deformed surfaces $\Gamma(\tau)$ and may be differentiated with respect to τ in $\tau = 0$. This will turn out to be useful when computing the variation of the (local and non-local) membrane energies.

Lemma 2.3 (Derivative of the variational curvature equation [18]). *Let* $\{\boldsymbol{z}(\tau) : \Gamma(\tau) \to \mathbb{R}^3\}_\tau$ *be such that* $\partial^\bullet_\tau \boldsymbol{z}|_{\tau=0} = 0$. *Then*

$$0 = \frac{d}{d\tau}\left(\int_{\Gamma(\tau)} -\boldsymbol{H}(\tau)\cdot\boldsymbol{z}(\tau) + \nabla_{\Gamma(\tau)}\boldsymbol{x}(\tau) : \nabla_{\Gamma(\tau)}\boldsymbol{z}(\tau)\right)\Big|_{\tau=0} = \int_\Gamma -\partial^\bullet_\tau \boldsymbol{H}\cdot\boldsymbol{z} - \boldsymbol{H}\cdot\boldsymbol{z}\nabla_\Gamma\cdot\boldsymbol{w}$$
$$+ \int_\Gamma \nabla_\Gamma \boldsymbol{z} : \nabla_\Gamma \boldsymbol{w} + \nabla_\Gamma\cdot\boldsymbol{z}\nabla_\Gamma\cdot\boldsymbol{w} - (\nabla_\Gamma\boldsymbol{z})^T : \nabla_\Gamma\boldsymbol{w} - \boldsymbol{P}\nabla_\Gamma\boldsymbol{z} : \nabla_\Gamma\boldsymbol{w} \tag{2.5}$$

Proof. This lemma has been shown in [18]. For the readers convenience, we repeat the proof here. Applying (A.9) to the first term of (A.3) and using $\partial^\bullet_\tau \boldsymbol{z} = 0$ we obtain

$$\frac{d}{d\tau}\int_{\Gamma(\tau)} \boldsymbol{H}(\tau)\cdot\boldsymbol{z}(\tau)|_{\tau=0} = \int_\Gamma \partial^\bullet_\tau\boldsymbol{H}\cdot\boldsymbol{z} + \boldsymbol{H}\cdot\boldsymbol{z}\nabla_\Gamma\cdot\boldsymbol{w}$$

For the second term of (A.3) we apply the Leibniz formula involving surface gradients (A.10):

$$\frac{d}{d\tau}\int_{\Gamma(\tau)} \nabla_{\Gamma(\tau)}\boldsymbol{x}(\tau) : \nabla_{\Gamma(\tau)}\boldsymbol{z}(\tau)\Big|_{\tau=0} = \frac{d}{d\tau}\int_{\Gamma(\tau)}\sum_i \nabla_{\Gamma(\tau)}\boldsymbol{x}_i(\tau)\cdot\nabla_{\Gamma(\tau)}\boldsymbol{z}_i(\tau)\Big|_{\tau=0}$$
$$= \int_\Gamma \sum_i \nabla_\Gamma\partial^\bullet_\tau\boldsymbol{x}_i\cdot\nabla_\Gamma\boldsymbol{z}_i + \nabla_\Gamma\boldsymbol{x}_i\cdot\nabla_\Gamma\partial^\bullet_\tau\boldsymbol{z}_i + \int_\Gamma\sum_i \nabla_\Gamma\boldsymbol{x}_i\cdot(\nabla_\Gamma\cdot\boldsymbol{w} - 2D(\boldsymbol{w}))\nabla_\Gamma\boldsymbol{z}_i$$

and with the identities $\partial^\bullet_\tau\boldsymbol{x} = \boldsymbol{w}$ (the time t is replaced by τ and the deformation field $\boldsymbol{w}$ is the velocity field), $\partial^\bullet_\tau\boldsymbol{z} = 0$, $\nabla_\Gamma\boldsymbol{x} : \nabla_\Gamma\boldsymbol{z} = \nabla_\Gamma\cdot\boldsymbol{z}$ and (A.11) we get

$$= \int_\Gamma \sum_i (\nabla_\Gamma\boldsymbol{w}_i\cdot\nabla_\Gamma\boldsymbol{z}_i) + \nabla_\Gamma\boldsymbol{x} : \nabla_\Gamma\boldsymbol{z}\nabla_\Gamma\cdot\boldsymbol{w} - \sum_i(\nabla_\Gamma\boldsymbol{x}_i\cdot 2D(\boldsymbol{w})\nabla_\Gamma\boldsymbol{z}_i)$$
$$= \int_\Gamma \nabla_\Gamma\boldsymbol{z} : \nabla_\Gamma\boldsymbol{w} + \nabla_\Gamma\cdot\boldsymbol{z}\nabla_\Gamma\cdot\boldsymbol{w} - (\nabla_\Gamma\boldsymbol{z})^T : \nabla_\Gamma\boldsymbol{w} - \boldsymbol{P}\nabla_\Gamma\boldsymbol{z} : \nabla_\Gamma\boldsymbol{w}$$

Please cite this article in press as: C.M. Elliott, B. Stinner, Modeling and computation of two phase geometric biomembranes using surface finite elements, J. Comput. Phys. (2010), doi:10.1016/j.jcp.2010.05.014

Taking both derived identities together we end up with (2.5). □

In a series of lemmas we now present the variations of several contributions to the energy functional.

Lemma 2.4 (Variation of the Willmore functional [18]). *The variation of the bending energy functional is:*

$$\langle D\mathcal{F}_W(\Gamma), \boldsymbol{w}\rangle = \int_\Gamma -\frac{k_H}{2}|\boldsymbol{H}|^2\nabla_\Gamma\cdot\boldsymbol{w} + k_H\nabla_\Gamma\boldsymbol{H}:\nabla_\Gamma\boldsymbol{w} + k_H\nabla_\Gamma\cdot\boldsymbol{H}\nabla_\Gamma\cdot\boldsymbol{w} - \int_\Gamma k_H(\nabla_\Gamma\boldsymbol{H})^T:\nabla_\Gamma\boldsymbol{w} + k_H\boldsymbol{P}\nabla_\Gamma\boldsymbol{H}:\nabla_\Gamma\boldsymbol{w} \tag{2.6}$$

Proof. Also this lemma has already been shown in [18]. Using (A.9) we see that

$$\frac{d}{d\tau}\mathcal{F}_W(\Gamma(\tau))\Big|_{\tau=0} = \int_\Gamma k_H\partial_\tau^\bullet\boldsymbol{H}\cdot\boldsymbol{H} + \frac{k_H}{2}|\boldsymbol{H}|^2\nabla_\Gamma\cdot\boldsymbol{w} \tag{2.7}$$

We now employ Lemma 2.3 with a field z which for $\tau = 0$ coincides with H and, as required, fulfills $\partial_\tau^\bullet z|_{\tau=0} = 0$. From (2.5) we obtain that

$$\int_\Gamma \partial_\tau^\bullet\boldsymbol{H}\cdot\boldsymbol{H} = \int_\Gamma(-|\boldsymbol{H}|^2\nabla_\Gamma\cdot\boldsymbol{w} + \nabla_\Gamma\boldsymbol{H}:\nabla_\Gamma\boldsymbol{w}) + \int_\Gamma(\nabla_\Gamma\cdot\boldsymbol{H}\nabla_\Gamma\cdot\boldsymbol{w} - (\nabla_\Gamma\boldsymbol{H})^T:\nabla_\Gamma\boldsymbol{w} - \boldsymbol{P}\nabla_\Gamma\boldsymbol{H}:\nabla_\Gamma\boldsymbol{w})$$

Multiplying with k_H and replacing the first term in (2.7) we deduce (2.6). □

Remark 2.5. The formula for the variation of the bending energy $\mathcal{F}_W$ usually reads

$$\frac{d}{d\tau}\mathcal{F}_W(\Gamma(\tau))\Big|_{\tau=0} = k_H\int_\Gamma\left(-\Delta_\Gamma H - |\nabla_\Gamma\boldsymbol{v}|^2H + \frac{1}{2}H^3\right)\boldsymbol{v}\cdot\boldsymbol{w} \tag{2.8}$$

see e.g. [40] for a derivation. In particular, only deformations in the normal direction have an impact on the bending energy, which is clear since purely tangential deformations do not change the surface. With some lengthy calculations involving integrations by parts one can deduce this from (2.6). For the numerics we will make use of the variational formulation (2.6) but (2.8) is useful for the asymptotic analysis of the governing equations [22].

Lemma 2.6 (Variation of the non-local bending energy functional). *The variation of the non-local bending energy functional is:*

$$\langle D\mathcal{F}_M(\Gamma), \boldsymbol{w}\rangle = \int_\Gamma \frac{k_H\alpha}{8\bar{R}}(m-m_0)(|\nabla_\Gamma\cdot\boldsymbol{v}|^2 - |\nabla_\Gamma\boldsymbol{v}|^2)\boldsymbol{v}\cdot\boldsymbol{w}. \tag{2.9}$$

Proof. In order to compute the variation of the non-local bending energy (1.5) we first observe that

$$\frac{d}{d\tau}\int_{\Gamma(\tau)}\boldsymbol{H}(\tau)\cdot\boldsymbol{v}(\tau)\Big|_{\tau=0} = \int_\Gamma \partial_\tau^\bullet\boldsymbol{H}\cdot\boldsymbol{v} + \boldsymbol{H}\cdot\partial_\tau^\bullet\boldsymbol{v} + \underbrace{\boldsymbol{H}\cdot\boldsymbol{v}}_{=H=\nabla_\Gamma\cdot\boldsymbol{v}}\underbrace{\nabla_\Gamma\cdot\boldsymbol{w}}_{=\nabla_\Gamma\cdot\boldsymbol{v}\boldsymbol{w}} \tag{2.10}$$

where we used (A.9) again. For the first term we employ Lemma 2.3 with a field z which for $\tau = 0$ coincides with v. In the following calculation we use the symmetry of the tangential tensor $\nabla_\Gamma v$ which, in particular, means that $P\nabla_\Gamma v = P(\nabla_\Gamma v)^T = (\nabla_\Gamma v)^T = \nabla_\Gamma v$, and we further use that $\nabla_\Gamma w = w\nabla_\Gamma v + v\otimes\nabla_\Gamma w$ as well as (A.2).

$$\begin{aligned}\int_\Gamma \partial_\tau^\bullet\boldsymbol{H}\cdot\boldsymbol{v} &= \int_\Gamma \underbrace{-\boldsymbol{H}\cdot\boldsymbol{v}}_{=-H}\nabla_\Gamma\cdot\boldsymbol{w} + \nabla_\Gamma\boldsymbol{v}:\nabla_\Gamma\boldsymbol{w} + \underbrace{\nabla_\Gamma\cdot\boldsymbol{v}}_{=H}\nabla_\Gamma\cdot\boldsymbol{w} - \int_\Gamma(\nabla_\Gamma\boldsymbol{v})^T:\nabla_\Gamma\boldsymbol{w} + \boldsymbol{P}\nabla_\Gamma\boldsymbol{v}:\nabla_\Gamma\boldsymbol{w}\\ &= -\int_\Gamma\nabla_\Gamma\boldsymbol{v}:(w\nabla_\Gamma\boldsymbol{v} + \boldsymbol{v}\otimes\nabla_\Gamma w) = -\int_\Gamma|\nabla_\Gamma\boldsymbol{v}|^2w\end{aligned}$$

Recalling the identity (A.12) we have

$$\boldsymbol{H}\cdot\partial_\tau^\bullet\boldsymbol{v} = -\boldsymbol{H}\cdot(\nabla_\Gamma\boldsymbol{w})^T\boldsymbol{v} = -\nabla_\Gamma\boldsymbol{w}\boldsymbol{H}\cdot\boldsymbol{v} = 0$$

since H points in the normal direction, so the second term in (2.10) vanishes. Altogether this gives

$$\frac{d}{d\tau}\int_{\Gamma(\tau)}\boldsymbol{H}(\tau)\cdot\boldsymbol{v}(\tau)\Big|_{\tau=0} = \int_\Gamma -|\nabla_\Gamma\boldsymbol{v}|^2w + |\nabla_\Gamma\cdot\boldsymbol{v}|^2w = \int_\Gamma(-|\nabla_\Gamma\boldsymbol{v}|^2 + |\nabla_\Gamma\cdot\boldsymbol{v}|^2)\boldsymbol{v}\cdot\boldsymbol{w}.$$

From this and since

$$\frac{d}{d\tau}\mathcal{F}_M(\Gamma(\tau))\Big|_{\tau=0} = \frac{k_H\alpha}{8\bar{R}}(m-m_0)\frac{d}{d\tau}\int_{\Gamma(\tau)}\boldsymbol{H}(\tau)\cdot\boldsymbol{v}(\tau)\Big|_{\tau=0}$$

we conclude that (2.9) is true. □

Please cite this article in press as: C.M. Elliott, B. Stinner, Modeling and computation of two phase geometric biomembranes using surface finite elements, J. Comput. Phys. (2010), doi:10.1016/j.jcp.2010.05.014

As is well known, the variation of the enclosed volume is the external unit normal and the variation of the surface area is the mean curvature vector. This can also be deduced from the transport identity (A.9) with $\eta = 1$ for the area and $\eta = 1$ and Γ replaced by Ω for the volume.

Lemma 2.7. Variation of the area and volume functionals). *The variations of the volume and area constraint functional are:*

$$\langle D\mathcal{C}_V(\Gamma), \boldsymbol{w}\rangle = \int_\Gamma \boldsymbol{v}\cdot\boldsymbol{w}, \tag{2.11}$$

$$\langle D\mathcal{C}_A(\Gamma), \boldsymbol{w}\rangle = \int_\Gamma \boldsymbol{H}\cdot\boldsymbol{w} \overset{(A.3)}{=} \int_\Gamma \nabla_\Gamma \boldsymbol{x} : \nabla_\Gamma \boldsymbol{w} \tag{2.12}$$

2.3. Variations of phase field surface functionals

Given an admissible phase field surface, variations with respect to the surface are based on deformations which we will restrict to the normal direction. But when deforming we have to say how the phase field variable defined on the surface changes.

Definition 2.8. Admissible deformations of phase field surfaces). Given an admissible phase field surface (Γ, c), a smooth normal vector field $\boldsymbol{w} = w\boldsymbol{\nu} : \Gamma \to \mathbb{R}^3$ and a smooth function $\eta : \Gamma \to \mathbb{R}$, the *deformed admissible phase field surface $(\Gamma(\tau), c(\tau))$ in direction (w,η)* for a small $\tau \in \mathbb{R}$ is defined by

$$\Gamma(\tau) := \{\boldsymbol{x}(\tau) := \boldsymbol{x} + \tau w(\boldsymbol{x})\boldsymbol{\nu}(\boldsymbol{x}) | \boldsymbol{x} \in \Gamma\}, \tag{2.13}$$

$$c(\tau) : \Gamma(\tau) \to \mathbb{R}, \quad c(\tau, \boldsymbol{x}(\tau)) := c(\boldsymbol{x}) + \tau\eta(\boldsymbol{x}) \tag{2.14}$$

Such a pair (w,η) is called *admissible deformation field* for an admissible phase field surface.

By the regularity assumptions on admissible phase field surfaces there is a small $\tau_0 > 0$ so that $(\Gamma(\tau), c(\tau))$ indeed is admissible for all $\tau \in (-\tau_0, \tau_0)$. In particular, for each point $\boldsymbol{x}(\tau)$ on $\Gamma(\tau)$ there is a unique point $\boldsymbol{x} \in \Gamma$ with $\boldsymbol{x}(\tau) = \boldsymbol{x} + \tau w(\boldsymbol{x})\boldsymbol{\nu}(\boldsymbol{x})$ so that $c(\tau)$ is well defined. Concerning the derivative of $c(\tau)$ with respect to τ we observe that

$$\frac{d}{d\tau} c(\tau, \boldsymbol{x}(\tau))\Big|_{\tau=0} = \partial_\tau c(0, \boldsymbol{x}(0)) + \partial_\tau \boldsymbol{x}(0)\cdot\nabla c(0, \boldsymbol{x}(0)) = \partial_\tau c(0,\boldsymbol{x}) + w(\boldsymbol{x})\boldsymbol{\nu}(\boldsymbol{x})\cdot\nabla c(\boldsymbol{x}) = \partial_\tau^\circ c(\tau, \boldsymbol{x}(\tau))|_{\tau=0}$$

where we employed the notation of Section A.2 with t replaced by the parameter τ. On the other hand, from (2.14) we see that $\frac{d}{d\tau} c(\tau, \boldsymbol{x}(\tau))|_{\tau=0} = \eta(\boldsymbol{x})$, whence

$$\partial_\tau^\bullet c(\tau, \boldsymbol{x}(\tau))|_{\tau=0} = \partial_\tau^\circ c(\tau, \boldsymbol{x}(\tau))|_{\tau=0} = \eta(\boldsymbol{x}) \tag{2.15}$$

In the case $\eta = 0$ this means that we extend the phase field constantly in the normal direction away from Γ in order to define it on the deformed surface $\Gamma(\tau)$.

Definition 2.9. Let $\mathcal{E} = \mathcal{E}(\Gamma, c)$ be a functional defined on admissible phase field surfaces, let (Γ, c) be an admissible surface and let (w,η) be an admissible deformation field. The variation of $\mathcal{E}$ in (Γ, c) in direction (w,η) is defined by

$$\langle \delta\mathcal{E}(\Gamma, c), (w,\eta)\rangle = \frac{d}{d\tau}\mathcal{E}(\Gamma(\tau), c(\tau))\Big|_{\tau=0}$$

Remark 2.10. We will also be interested in variations of functionals that only depend on Γ but not on c, namely $\mathcal{F}_W, \mathcal{F}_M, \mathcal{C}_A$, and $\mathcal{C}_V$. With a slight abuse of notation we will still write $\delta\mathcal{F}_W$ etc. where we mean

$$\langle \delta\mathcal{F}_W(\Gamma), (w,\eta)\rangle := \langle D\mathcal{F}_W(\Gamma), w\boldsymbol{\nu}\rangle \tag{2.16}$$

Lemma 2.11 (Variation of the Ginzburg–Landau energy functional). *For an admissible phase field surface (Γ, c) with admissible deformation field (w,η) we have that*

$$\langle \delta\mathcal{F}_{GL}(\Gamma, c), (w,\eta)\rangle = \int_\Gamma \sigma\left(\varepsilon\nabla_\Gamma c\cdot\nabla_\Gamma\eta + \frac{1}{\varepsilon}W'(c)\eta\right) - \int_\Gamma \sigma\varepsilon\nabla_\Gamma c\otimes\nabla_\Gamma c : \nabla_\Gamma \boldsymbol{\nu} w + \int_\Gamma \sigma\left(\frac{\varepsilon}{2}|\nabla_\Gamma c|^2 + \frac{1}{\varepsilon}W(c)\right)Hw, \tag{2.17}$$

Proof. Thanks to (A.2)

$$\nabla_\Gamma\cdot\boldsymbol{w} = \nabla_\Gamma\cdot(w\boldsymbol{\nu}) = w\nabla_\Gamma\cdot\boldsymbol{\nu} + \underbrace{\nabla_\Gamma w\cdot\boldsymbol{\nu}}_{=0} = wH$$

Furthermore, using the symmetry of $\nabla_\Gamma\nu$ again,

Please cite this article in press as: C.M. Elliott, B. Stinner, Modeling and computation of two phase geometric biomembranes using surface finite elements, J. Comput. Phys. (2010), doi:10.1016/j.jcp.2010.05.014

$$2D(\boldsymbol{w}) = \nabla_\Gamma(w\boldsymbol{v}) + (\nabla_\Gamma(w\boldsymbol{v}))^T = 2w\nabla_\Gamma \boldsymbol{v} + \nabla_\Gamma w \otimes \boldsymbol{v} + \boldsymbol{v} \otimes \nabla_\Gamma w$$

Applying (A.10) to the term involving $\nabla_\Gamma c$ we obtain

$$\begin{aligned}\frac{d}{d\tau}\int_{\Gamma(\tau)} \frac{\sigma\varepsilon}{2}|\nabla_{\Gamma(\tau)}c(\tau)|^2\Big|_{\tau=0} &= \int_\Gamma \sigma\varepsilon\nabla_\Gamma c\cdot\nabla_\Gamma\partial_\tau^\bullet c + \frac{\sigma\varepsilon}{2}\nabla_\Gamma c\cdot(\nabla_\Gamma\cdot\boldsymbol{w} - 2D(\boldsymbol{w}))\nabla_\Gamma c\\ &= \int_\Gamma \sigma\varepsilon\nabla_\Gamma c\cdot\nabla_\Gamma\eta + \frac{\sigma\varepsilon}{2}|\nabla_\Gamma c|^2 Hw - \sigma\varepsilon\nabla_\Gamma c\otimes\nabla_\Gamma c : \nabla_\Gamma \boldsymbol{v} w\\ &\quad - \int_\Gamma \frac{\sigma\varepsilon}{2}\underbrace{\nabla_\Gamma c\cdot(\nabla_\Gamma w\otimes\boldsymbol{v} + \boldsymbol{v}\otimes\nabla_\Gamma w)\nabla_\Gamma c}_{=0\text{since}\nabla_\Gamma c\cdot\boldsymbol{v}=0}\end{aligned}$$

Similarly, applying (A.9) to the term with the double well potential we obtain

$$\frac{d}{d\tau}\int_{\Gamma(\tau)}\frac{\sigma}{\varepsilon}W(c(\tau))\Big|_{\tau=0} = \int_\Gamma \frac{\sigma}{\varepsilon}W'(c)\partial_\tau^\bullet c + \frac{\sigma}{\varepsilon}W(c)\nabla_\Gamma\cdot\boldsymbol{w} = \int_\Gamma \frac{\sigma}{\varepsilon}W'(c)\eta + W(c)Hw$$

Both together yields (2.17):

$$\frac{d}{d\tau}\mathcal{F}_{GL}(\Gamma(\tau),c(\tau))\Big|_{\tau=0} = \sigma\int_\Gamma \varepsilon\nabla_\Gamma c\cdot\nabla_\Gamma\eta + \frac{1}{\varepsilon}W'(c)\eta - \varepsilon\nabla_\Gamma c\otimes\nabla_\Gamma c : \nabla_\Gamma \boldsymbol{v} w + \sigma\int_\Gamma\left(\frac{\varepsilon}{2}|\nabla_\Gamma c|^2 + \frac{1}{\varepsilon}W(c)\right)Hw \qquad \square$$

Lemma 2.12 (Variation of the mass constraint functional). *For an admissible phase field surface (Γ,c) with admissible deformation field (w,η) we have that*

$$\langle\delta\mathcal{C}_c(\Gamma,c),(w,\eta)\rangle = \int_\Gamma h'(c)\eta + h(c)Hw \tag{2.18}$$

Proof. We use (A.9), (2.15) and (A.2):

$$\langle\delta\mathcal{C}_c(\Gamma,c),(w,\eta)\rangle = \frac{d}{d\tau}\left(\int_{\Gamma(\tau)}h(c(\tau))\right)\Big|_{\tau=0} = \int_\Gamma h'(c)\partial_t^\bullet c + h(c)\nabla_\Gamma\cdot(w\boldsymbol{v}) = \int_\Gamma h'(c)\eta + h(c)Hw$$

which is the desired formula. $\square$

2.4. Critical points

2.4.1. Diffuse interface model

Definition 2.13 (*Critical point, diffuse interface model*). An admissible phase field surface (Γ,c) is a *critical point* of the diffuse interface membrane energy (1.2) subject to constraints 2.2, 2.3 and 2.4 if

$$0 = (\delta\mathcal{F}_W + \delta\mathcal{F}_{GL} + \delta\mathcal{F}_M + \lambda_V\delta\mathcal{C}_V + \lambda_A\delta\mathcal{C}_A + \lambda_c\delta\mathcal{C}_c)(\Gamma,c)$$

where λ_V, λ_A, and λ_c are appropriate Lagrange multipliers.

Using (2.8), (2.17), (2.9), (2.11), (2.12) and (2.18) and recalling (2.16) critical points have to fulfill.

Problem 2.14 (*Diffuse interface equilibrium equations*). For given values V, A_1, A_2 fulfilling (2.1) find an admissible phase field surface (Γ,c) and Lagrange multipliers λ_V, λ_A, and λ_c such that

$$\begin{aligned}0 &= k_H\left(-\Delta_\Gamma H - |\nabla_\Gamma\boldsymbol{\nu}|^2 H + \frac{1}{2}H^3\right) - \sigma\varepsilon\nabla_\Gamma c\otimes\nabla_\Gamma c : \nabla_\Gamma\boldsymbol{\nu} + \left(\frac{\sigma\varepsilon}{2}|\nabla_\Gamma c|^2 + \frac{\sigma}{\varepsilon}W(c)\right)H\\ &\quad + \frac{k_H\alpha}{4\bar{R}}(m-m_0)(H^2 - |\nabla_\Gamma\boldsymbol{\nu}|^2) + \lambda_V + (\lambda_A + \lambda_c h(c))H,\end{aligned} \tag{2.19}$$

$$0 = -\varepsilon\sigma\Delta_\Gamma c + \frac{\sigma}{\varepsilon}W'(c) + \lambda_c h'(c), \tag{2.20}$$

$$0 = |\Omega| - V, \quad 0 = |\Gamma| - (A_1 + A_2), 0 = \int_\Gamma h(c) - (A_1 - A_2) \tag{2.21}$$

Please cite this article in press as: C.M. Elliott, B. Stinner, Modeling and computation of two phase geometric biomembranes using surface finite elements, J. Comput. Phys. (2010), doi:10.1016/j.jcp.2010.05.014

First equation (2.19) can be understood as a normal force balance whilst (2.20) is a kind of tangential force balance. This will become more clear when comparing with the equilibrium equations in the sharp interface limit in Problem 2.16 below which we provide some interpretation of equations. Remark 2.17 explains the relation between the above diffuse interface problem and the sharp interface problem.

2.4.2. Sharp interface model

Definition 2.15 (*Admissible two-phase surface*). For the membrane energy (1.4) Γ is an *admissible two-phase surface* if it is the boundary of a bounded, simply connected open domain $\Omega \subset \mathbb{R}^3$ such that Γ is C^1-diffeomorphic to the sphere and such that it can be decomposed in the form $\Gamma = \Gamma_1 \cup \gamma \cup \Gamma_2$ where

- Γ_1 and Γ_2 are two-dimensional smooth oriented not necessarily connected hypersurfaces with smooth boundaries that coincide and correspond to γ which consists of a finite number of smooth curves,
  $\partial\Gamma_1 = \partial\Gamma_2 = \gamma$,
- locally around each point $x \in \gamma$ the surface Γ can be parameterized by a C^1 map.

These regularity assumptions are consistent with the approach in [31,32,4]. The fact that the lipid bilayer is intact across the phase interface motivates the assumption of a C^1 surface (see the discussion in [31]).

For the admissible two-phase surface $\Gamma = \Gamma_1 \cup \gamma \cup \Gamma_2$ we denote by $\boldsymbol{\mu}$ the outer co-normal of Γ_2, whence $-\boldsymbol{\mu}$ is the outer co-normal of Γ_1. We also use $\boldsymbol{\tau}_\gamma$ for the unit tangential vector field along γ such that $(\boldsymbol{\tau}_\gamma, \boldsymbol{\mu}, \boldsymbol{\nu})$ is positively oriented.

The Euler–Lagrange equations of the membrane energy (1.4) can be derived by deforming the surface Γ with a suitably regular vector field. The calculation is carried out in [22] for more general energies.

Problem 2.16 (*Sharp interface equilibrium equations*). For given data $\{V, A_1, A_2\}$ fulfilling (2.1) find an admissible two-phase membrane $\Gamma = \Gamma_1 \cup \gamma \cup \Gamma_2$ and find Lagrange multipliers λ_V, $\lambda_{A,1}$, and $\lambda_{A,2}$ such that

$$0 = k_H(-\Delta_{\Gamma_i} H^{(i)} - |\nabla_{\Gamma_i}\boldsymbol{\nu}^{(i)}|^2 H^{(i)} + \frac{1}{2}(H^{(i)})^3) + \frac{k_H\alpha}{4\bar{R}}(m - m_0)\Big((H^{(i)})^2 - |\nabla_{\Gamma_i}\boldsymbol{\nu}^{(i)}|^2\Big) + \lambda_V + \lambda_{A,i} H \quad \text{on } \Gamma_i,\ i = 1,2, \tag{2.22}$$

$$0 = k_H[H]_2^1 \quad \text{on } \gamma, \tag{2.23}$$

$$0 = k_H[\nabla_\Gamma H]_2^1 \cdot \boldsymbol{\mu} - \bar{\sigma} h_\nu \quad \text{on } \gamma, \tag{2.24}$$

$$0 = \bar{\sigma} h_g + (\lambda_{A,2} - \lambda_{A,1}) \quad \text{on } \gamma, \tag{2.25}$$

$$0 = |\Omega| - V, \tag{2.26}$$

$$0 = |\Gamma_i| - A_i,\ i = 1,2. \tag{2.27}$$

Eq. (2.22) can be considered as a force balance in points on the membrane where we emphasize that forces arising from the bending energy and the constraints point in the normal direction so that we can formulate it as a scalar equation for the normal components of the forces. The phase interface involves both a continuity condition (2.23) and a force balance which is split into a component (2.25) tangential to Γ and normal to γ and a component (2.24) normal to Γ. Since the Lagrange multipliers are real numbers we see from (2.25) that equilibrium membrane shapes involve phase interfaces which all have the same constant geodesic curvature.

Remark 2.17. It is shown in [22] by a formal asymptotic analysis that solutions to Problem 2.14 converge to solutions to Problem 2.16 as $\varepsilon \to 0$. Here, we confine ourselves to making a few remarks for readers that are familiar with this technique.

- Energetically favorable solutions to the Allen–Cahn equations involve large domains where $c \approx \pm 1$ which correspond to the phases Γ_i in the sharp interface limit. With this in mind we see how (2.22) emerges from (2.19).
- These equations also allow us to identify $\lambda_{A,1}$ with $\lambda_A + \lambda_c$ and $\lambda_{A,2}$ with $\lambda_A - \lambda_c$ in the sharp interface limit, $\epsilon \to 0$.
- The term $\varepsilon\Delta_\Gamma c - \frac{1}{\varepsilon}W'(c)$ converges to the geodesic curvature h_g of the limiting curve γ which allows us to recover (2.25) from (2.20).
- The curvature terms in (2.23) and (2.24) arise from the expansion of the term $\Delta_\Gamma H$ in (2.19) in the interfacial layer between the phases. The normal component of curvature h_ν is obtained from the second line of (2.19) which to leading order approximates $\sim \frac{1}{\varepsilon}\bar{\sigma}(-\boldsymbol{\mu}\cdot\nabla_\Gamma\boldsymbol{\nu}\boldsymbol{\mu} + H)$ on γ since $\nabla_\Gamma c \sim \frac{1}{\varepsilon}\boldsymbol{\mu}$ there. Using the fact that (τ_γ, μ) is an orthonormal basis of the tangent space on Γ we may write $H = \nabla_\Gamma \cdot \nu = \mu \cdot \nabla_\Gamma \nu\mu + \tau_\gamma \cdot \nabla_\Gamma \nu\tau_\gamma$ and obtain h_ν by observing that $\tau_\gamma \cdot \nabla_\Gamma \nu\tau_\gamma = h_\nu$.

2.5. Relaxation dynamics and energy decay

We define a relaxation dynamics as a weighted L^2 gradient flow of the membrane energy taking the constraints into account with Lagrange multipliers.

Please cite this article in press as: C.M. Elliott, B. Stinner, Modeling and computation of two phase geometric biomembranes using surface finite elements, J. Comput. Phys. (2010), doi:10.1016/j.jcp.2010.05.014

Definition 2.18 (*Weighted L^2 product*). Let (Γ,c) denote an admissible phase field surface and let $\omega>0$ be a kinetic coefficient. On the space of admissible deformation fields we consider the inner product

$$\mathcal{M}_\omega((v,\chi),(w,\eta);(\Gamma,c)) := \int_\Gamma (vw+\varepsilon\omega\chi\eta).$$

The kinetic coefficient ω yields a time scale which may speed up or slow down the phase separation in comparison with the membrane surface relaxation. We remark that we will end up with an Allen–Cahn equation for the order parameter c on the evolving surface Γ which, with the ϵ scaling of the kinetic coefficien,t will approximate a forced geodesic curvature flow for the interphase line in the sharp interface limit. We chose it in analogy with the phase field approximation of mean curvature flow in flat domains [13,25].

Problem 2.19 (*Gradient flow*). Suppose that data $\{V,A_1,A_2\}$ fulfilling (2.1) and an initial admissible phase field surface (Γ^0,c^0) are given such that

$$V=|\Omega^0|=\frac{1}{3}\int_{\Gamma^0}\boldsymbol{v}^0\cdot\boldsymbol{x}^0,\quad A_1+A_2=|\Gamma^0|,\quad A_1-A_2=\int_{\Gamma^0}h(c^0). \tag{2.28}$$

Find a family of admissible phase field surfaces $\{(\Gamma(t),cc(t))\}_{t\in[0,\infty)}$ that satisfy $(\Gamma(0),c(0))=(\Gamma^0,c^0)$ and have the velocity $v(t)=v_v(t)\nu(t)$ of $\Gamma(t)$, and find functions $\lambda_V,\lambda_A,\lambda_c:[0,\infty)\to\mathbb{R}$ such that at each time $t\in[0,\infty)$

$$\mathcal{M}_\omega((v_v(t),\partial_t^\bullet c(t)),(w,\eta);\quad(\Gamma(t),c(t))) \tag{2.29}$$
$$=-\langle(\delta\mathcal{F}_W+\delta\mathcal{F}_{GL}+\delta\mathcal{F}_M)(\Gamma(t),c(t)),(w,\eta)\rangle \tag{2.30}$$
$$-\langle(\lambda_V(t)\delta\mathcal{C}_V+\lambda_A(t)\delta\mathcal{C}_A+\lambda_c(t)\delta\mathcal{C}_c)(\Gamma(t),c(t)),(w,\eta)\rangle \tag{2.31}$$

for all admissible deformations (w,η) of $(\Gamma(t),c(t))$, and such that at each time $t\in[0,\infty)$

$$0=\mathcal{C}_V(\Gamma(t),c(t)), \tag{2.32}$$
$$0=\mathcal{C}_A(\Gamma(t),c(t)), \tag{2.33}$$
$$0=\mathcal{C}_c(\Gamma(t),c(t)). \tag{2.34}$$

Theorem 2.20. *Suppose that $\{(\Gamma(t),c(t)),\lambda_V(t),\lambda_A(t),\lambda_c(t)\}_t$ is a solution to Problem 2.19. Then*

$$\frac{d}{dt}\mathcal{F}(\Gamma(t),c(t))=-\int_{\Gamma(t)}(|v_v(t)|^2+\varepsilon\omega|\partial_t^\bullet c(t)|^2)\leqslant 0. \tag{2.35}$$

Proof. Thanks to the Lagrange multipliers the solution satisfies

$$0=\frac{d}{dt}\mathcal{C}_V(\Gamma(t),c(t))=\langle\delta\mathcal{C}_V(\Gamma(t),c(t)),(v_v(t),\partial_t^\bullet c(t))\rangle,$$
$$0=\frac{d}{dt}\mathcal{C}_A(\Gamma(t),c(t))=\langle\delta\mathcal{C}_A(\Gamma(t),c(t)),(v_v(t),\partial_t^\bullet c(t))\rangle,$$
$$0=\frac{d}{dt}\mathcal{C}_c(\Gamma(t),c(t))=\langle\delta\mathcal{C}_c(\Gamma(t),c(t)),(v_v(t),\partial_t^\bullet c(t))\rangle.$$

Therefore

$$\begin{aligned}\frac{d}{dt}\mathcal{F}(\Gamma(t),c(t))&=\langle(\delta\mathcal{F}_W+\delta\mathcal{F}_{GL}+\delta\mathcal{F}_M)(\Gamma(t),c(t)),(v_v(t),\partial_t^\bullet c(t))\rangle\\&=\langle(\delta\mathcal{F}_W+\delta\mathcal{F}_{GL}+\delta\mathcal{F}_M+)(\Gamma(t),c(t)),(v_v(t),\partial_t^\bullet c(t))\rangle+\langle(\lambda_V(t)\delta\mathcal{C}_V+\lambda_A(t)\delta\mathcal{C}_A\\&\quad+\lambda_c(t)\delta\mathcal{C}_c)(\Gamma(t),c(t)),(v_v(t),\partial_t^\bullet c(t))\rangle\\&=-\mathcal{M}_\omega((v_v(t),\partial_t^\bullet c(t)),(v_v(t),\partial_t^\bullet c(t));(\Gamma(t),c(t)))\end{aligned}$$

from which the assertion follows. □

2.6. Relaxation flow

We now present the problem on which the numerical method will be based. Analytically, the L^2 relaxation flow defined below and the gradient flow dynamics in Problem 2.19 are equivalent since the right hand side of law (2.36) for the velocity points into the normal direction.

Problem 2.21 (*Strong form of relaxation flow*). Suppose that data $\{V,A_1,A_2\}$ fulfilling (2.1) and an initial admissible phase field surface (Γ^0,c^0) are given such that (2.28) is satisfied. Find a family of admissible phase field surfaces $\{(\Gamma(t),c(t))\}_{t\in[0,\infty)}$ with $(\Gamma(0),c(0))=(\Gamma^0,c^0)$ and with velocity $v(t)$ of $\Gamma(t)$, and find functions $\lambda_V,\lambda_A,\lambda_c:[0,\infty)\to\mathbb{R}$ such that at all times t

Please cite this article in press as: C.M. Elliott, B. Stinner, Modeling and computation of two phase geometric biomembranes using surface finite elements, J. Comput. Phys. (2010), doi:10.1016/j.jcp.2010.05.014

$$\boldsymbol{v} = k_H\Big(\Delta_\Gamma H + |\nabla_\Gamma \boldsymbol{v}|^2 H - \frac{1}{2}H^2\Big)\boldsymbol{v} + \sigma\varepsilon\nabla_\Gamma c\otimes\nabla_\Gamma c : \nabla_\Gamma \boldsymbol{v}\boldsymbol{v} - \Big(\frac{\sigma\varepsilon}{2}|\nabla_\Gamma c|^2 + \frac{\sigma}{\varepsilon}W(c)\Big)\boldsymbol{H}$$
$$+\frac{k_H\alpha}{4\overline{R}}(m-m_0)(|\nabla_\Gamma \boldsymbol{v}|^2 - H^2)\boldsymbol{v} - \lambda_V\boldsymbol{v} - (\lambda_A + \lambda_c h(c))\boldsymbol{H}, \tag{2.36}$$

such that

$$\varepsilon\omega\partial_t^\bullet c = \varepsilon\sigma\Delta_\Gamma c - \frac{\sigma}{\varepsilon}W'(c) - \lambda_c h'(c), \tag{2.37}$$

and such that the constraints (2.32)–(2.34) are fulfilled.

In order to formulate the above flow it in a variational form appropriate for surface finite elements we introduce for future convenience the following **variational forms**:

$$\mathcal{L}_s(\Gamma;\eta,\phi) := \int_\Gamma \eta\phi,$$
$$\mathcal{L}(\Gamma;\boldsymbol{z},\boldsymbol{w}) := \int_\Gamma \boldsymbol{z}\cdot\boldsymbol{w},$$
$$\mathcal{E}_s(\Gamma;\eta,\phi) = \int_\Gamma \nabla_\Gamma\eta\cdot\nabla_\Gamma\phi,$$
$$\mathcal{E}(\Gamma;\boldsymbol{z},\boldsymbol{w}) = \int_\Gamma \nabla_\Gamma\boldsymbol{z} : \nabla_\Gamma\boldsymbol{w},$$
$$\mathcal{R}(\Gamma;\boldsymbol{z},\boldsymbol{w}) = \int_\Gamma \nabla_\Gamma\cdot\boldsymbol{z}\nabla_\Gamma\cdot\boldsymbol{w} - (\nabla_\Gamma\boldsymbol{z})^T : \nabla_\Gamma\boldsymbol{w} + \boldsymbol{P}\nabla_\Gamma\boldsymbol{z} : \nabla_\Gamma\boldsymbol{w},$$
$$\mathcal{D}(\Gamma;\boldsymbol{z},\boldsymbol{w}) = \int_\Gamma \frac{1}{2}|\boldsymbol{z}|^2\nabla_\Gamma\cdot\boldsymbol{w},$$
$$\mathcal{W}(\Gamma;\boldsymbol{z},\boldsymbol{w}) = k_H\mathcal{E}(\Gamma;\boldsymbol{z},\boldsymbol{w}) + k_H\mathcal{R}(\Gamma;\boldsymbol{z},\boldsymbol{w}) + k_H\mathcal{D}(\Gamma;\boldsymbol{z},\boldsymbol{w}),$$
$$\mathcal{G}_1(\Gamma;\eta,\boldsymbol{Q},\boldsymbol{w}) = \int_\Gamma -\sigma\varepsilon\nabla_\Gamma\eta\otimes\nabla_\Gamma\eta : \boldsymbol{Q}\boldsymbol{v}\cdot\boldsymbol{w},$$
$$\mathcal{G}_2(\Gamma;\eta,\boldsymbol{z},\boldsymbol{w}) = \int_\Gamma \Big(\frac{\sigma\varepsilon}{2}|\nabla_\Gamma\eta|^2 + \frac{\sigma}{\varepsilon}W(\eta)\Big)(\boldsymbol{z}\cdot\boldsymbol{v})\boldsymbol{v}\cdot\boldsymbol{w}$$
$$\mathcal{M}_1(\Gamma;\boldsymbol{z}) = \frac{k_H\alpha}{4\overline{R}}\Big(\frac{1}{\overline{R}}\int_\Gamma \boldsymbol{z}\cdot\boldsymbol{v} - m_0\Big),$$
$$\mathcal{M}_2(\Gamma;\boldsymbol{Q},\boldsymbol{w}) = \int_\Gamma \Big(|\boldsymbol{Q}|^2 - |\mathrm{tr}(\boldsymbol{Q})|^2\Big)\boldsymbol{v}\cdot\boldsymbol{w},$$
$$\mathcal{N}(\Gamma;\boldsymbol{w}) = \int_\Gamma \boldsymbol{v}\cdot\boldsymbol{w},$$

where η, ϕ are scalar fields, $\boldsymbol{w}$, $\boldsymbol{z}$ are vector-valued fields, and $\boldsymbol{Q}$ is a tensor-valued field on Γ.

Problem 2.22. Variational relaxation flowSuppose that data $\{V,A_1,A_2\}$ fulfilling (2.1) and an initial admissible phase field surface (Γ^0,c^0) are given such that (2.28) is satisfied. Find a family of admissible phase field surfaces $\{(\Gamma(t),c(t))\}_{t\in[0,\infty)}$ with $(\Gamma(0),c(0)) = (\Gamma^0,c^0)$ and with velocity $v(t)$ of $\Gamma(t)$, and find functions $\lambda_V,\lambda_A,\lambda_c : [0,\infty)\to\mathbb{R}$ such that at all times t

$$\mathcal{L}(\Gamma;\boldsymbol{v},\boldsymbol{w}) = -\mathcal{W}(\Gamma;\boldsymbol{H},\boldsymbol{w}) - \mathcal{G}_1(\Gamma;c,\nabla_\Gamma\boldsymbol{v},\boldsymbol{w}) - \mathcal{G}_2(\Gamma;c,\boldsymbol{H},\boldsymbol{w}) - \mathcal{M}_1(\Gamma;\boldsymbol{H})\mathcal{M}_2(\Gamma;\nabla_\Gamma\boldsymbol{v},\boldsymbol{w}) - \lambda_V\mathcal{N}(\Gamma;\boldsymbol{w})$$
$$-\lambda_A\mathcal{L}(\Gamma;\boldsymbol{H},\boldsymbol{w}) - \lambda_c\mathcal{L}(\Gamma;h(c)\boldsymbol{H},\boldsymbol{w}), \tag{2.38}$$

$$\omega\varepsilon\mathcal{L}_s(\Gamma;\partial_t^\bullet c,\phi) = -\varepsilon\sigma\mathcal{E}_s(\Gamma;c,\phi) - \frac{\sigma}{\varepsilon}\mathcal{L}_s(\Gamma;W'(c),\phi) - \lambda_c\mathcal{L}_s(\Gamma;h'(c),\phi) \tag{2.39}$$

for all test functions $(\boldsymbol{w},\phi) : \Gamma(t)\to\mathbb{R}^3\times\mathbb{R}$ where the fields $\{H(t)\}_t$ are computed from (A.3) and such that the constraints (2.32)–(2.34) are fulfilled.

3. Finite element approximation

We will use triangulated surfaces and surface finite elements in order to discretize the equations in Problem 2.22. For this purpose we need an approximation to the Weingarten map $\nabla_\Gamma\boldsymbol{v}$ which is given in Definition 3.5. In Section 3.2 we then present the spatial discretization and the fully discrete scheme in Definition 3.11. After, we describe the procedures to update surface, curvature and order parameter and state the solution algorithm.

Please cite this article in press as: C.M. Elliott, B. Stinner, Modeling and computation of two phase geometric biomembranes using surface finite elements, J. Comput. Phys. (2010), doi:10.1016/j.jcp.2010.05.014

3.1. Isoparametric quadratic surface finite elements

The discretization is based on triangulated surfaces and isoparametric surface finite elements. We refer to [27,10,14] for facts and results on such elements.

Definition 3.1 (Triangulated surface). A *triangulated polyhedral surface* $\widetilde{\Gamma}_h$ is a polyhedron with planar triangular faces,

$$\widetilde{\Gamma}_h = \bigcup_{\widetilde{T}\in\widetilde{\mathcal{T}}_h} \widetilde{T},$$

where $\widetilde{\mathcal{T}}_h$ consists of a finite number of closed, non-degenerate triangles $\widetilde{T}$ such that the intersection of two different triangles is either empty or a common edge or a common vertex and such that each triangle has at least one edge in common with another triangle.

Given a triangulated polyhedral surface $\widetilde{\Gamma}_h$, a *quadratic triangulated surface* Γ_h over $\widetilde{\Gamma}_h$ is of the form

$$\Gamma_h = \bigcup_{T\in\mathcal{T}_h} T,$$

where there exists a homeomorphism $\mathcal{F} : \widetilde{\Gamma}_h \to \Gamma_h$ such that

- for each $T \in \mathcal{T}_h$ there is a $\widetilde{T} \in \widetilde{\mathcal{T}}_h$ with $T = \mathcal{F}(\widetilde{T})$,
- $\mathcal{F}|_{\widetilde{T}}$ is a quadratic polynomial on each $\widetilde{T} \in \widetilde{\mathcal{T}}_h$,
- $\mathcal{F}$ leaves vertices unchanged.

It follows that each triangle $T \in \mathcal{T}_h$ can be parameterized by a quadratic polynomial $\Phi_T : \widehat{T} \to T$ where $\widehat{T} := \{\lambda \in \mathbb{R}^3 | \lambda_i \geqslant 0,\ \sum_i \lambda_i = 1\}$ is a fixed reference triangle. Denoting the space of polynomials of degree two by $\mathbb{P}^2(\cdot)$ we have that $\Phi_T \in \mathbb{P}^2(\widehat{T})$.

Definition 3.2. Isoparametric quadratic surface FE space Given a quadratic triangulated surface Γ_h, the *isoparametric quadratic surface finite element space* is defined by

$$S_h(\Gamma_h) := \{\phi \in C^0(\Gamma_h) | \phi|_T \circ \Phi_T \in \mathbb{P}^2(\widehat{T}) \text{ on each } T \in \mathcal{T}_h\}. \tag{3.1}$$

For discrete versions of three-dimensional fields such as, for example, the field $\boldsymbol{H} = \{\boldsymbol{H}_k\}_{k=1}^3$ we introduce the finite element space $\boldsymbol{S}_h(\Gamma_h) := S_h^3(\Gamma_h)$. We remark that the finite elements are isoparametric since the map $\mathcal{F}$ in Definition 3.1 belongs to $\boldsymbol{S}_h$. The matrix $\boldsymbol{P}_h = \boldsymbol{I} - \boldsymbol{\nu}_h \otimes \boldsymbol{\nu}_h = \nabla_{\Gamma_h} \boldsymbol{x}_h$ stands for the projection onto the tangential space of Γ_h and is well-defined at each point in the interior of a triangle $T \in \mathcal{T}_h$.

The nodal variables are the evaluations at the vertices and at the midpoints of the edges whose coordinates are denoted $\{\boldsymbol{x}_i\}_{i=1}^{N_h}$. Thus N_h is the dimension of S_h. We denote the standard basis by $\{\phi_i\}_{i=1}^{N_h}$ characterized by $\phi_i(\boldsymbol{x}_j) = \delta_{ij}$ with δ_{ij} being the Kronecker symbol. Elements $\zeta_h \in S_h$ can uniquely be written in the form $\zeta_h(\boldsymbol{x}) = \sum_i \zeta_i \phi_i(\boldsymbol{x})$ with coefficients $\zeta_i = \zeta_h(\boldsymbol{x}_i)$. We introduce the notation $\underline{\zeta} = (\zeta_i)_{i=1}^{N_h}$ for the coefficient vector. The standard basis of $\boldsymbol{S}_h^3$ is $\{\phi_i \boldsymbol{e}_k\}_{i,k=1}^{N_h,3}$ where $\boldsymbol{e}_k = \{\delta_{kj}\}_{j=1}^3$. We will employ the notation $\underline{\boldsymbol{H}} = \{\boldsymbol{H}_{i,k}\}_{i,k=1}^{N_h,3}$ where $\boldsymbol{H}_{i,k} = \boldsymbol{H}_h(\boldsymbol{x}_i) \cdot \boldsymbol{e}_k$.

Some of the functionals stated below involve the nonlinearities $W(\cdot)$ and $h(\cdot)$ and derivatives which are polynomials as long as $-1 \leqslant c_h \leqslant 1$. To compute the integrals we chose quadrature formulas that are exact for these polynomials.

Definition 3.3 (Discrete admissible phase field surface). A *discrete admissible phase field surface* (Γ_h, c_h) is a quadratic triangulated surface Γ_h of spherical topology that encloses a bounded, simply connected open domain Ω_h together with a scalar field $c_h \in S_h(\Gamma_h)$. For such discrete admissible phase field surfaces we denote the external unit normal of the enclosed Ω_h by ν_h and the identity on Γ_h by x_h.

It is convenient to generalize (A.3) to triangulated surfaces in order to define a finite element function representing the curvature on Γ_h:

Definition 3.4 (*Discrete variational curvature equation*). For a discrete admissible phase field surface (Γ_h, c_h) the *discrete mean curvature vector* $H_h \in S_h(\Gamma_h)$ is defined via

$$\mathcal{L}(\Gamma_h; \boldsymbol{H}_h, \boldsymbol{w}_h) - \mathcal{E}(\Gamma_h; \boldsymbol{x}_h, \boldsymbol{w}_h) = 0 \tag{3.2}$$

which has to hold for all $w_h \in S_h(\Gamma_h)$.

Formula (A.4) applied to the unit normal $\boldsymbol{\nu}$ on an admissible phase field surface yields

$$\int_\Gamma \nabla_\Gamma \boldsymbol{\nu} : \boldsymbol{Z} + \boldsymbol{\nu} \cdot (\nabla_\Gamma \cdot \boldsymbol{Z}) = \int_\Gamma \nabla_\Gamma \cdot (\boldsymbol{Z}^T \boldsymbol{\nu}) = \int_\Gamma (\boldsymbol{Z}^T \boldsymbol{\nu}) \cdot \boldsymbol{H}$$

for any smooth test function $\boldsymbol{Z} : \Gamma \to \mathbb{R}^{3\times 3}$ and motivates the following

Please cite this article in press as: C.M. Elliott, B. Stinner, Modeling and computation of two phase geometric biomembranes using surface finite elements, J. Comput. Phys. (2010), doi:10.1016/j.jcp.2010.05.014

Definition 3.5 (*Discrete Weingarten map*). For a discrete admissible phase field surface (Γ_h, c_h) with the discrete mean curvature vector satisfying (3.2) the *discrete Weingarten map* $\mathbf{Q}_h \in S_h^{3\times 3}(\Gamma_h)$ is defined via

$$\int_{\Gamma_h} \mathbf{Q}_h : \mathbf{Z}_h = -\int_{\Gamma_h} (\nabla_{\Gamma_h} \cdot \mathbf{Z}_h)\cdot \boldsymbol{\nu}_h + \int_{\Gamma_h} \boldsymbol{\nu}_h \otimes \boldsymbol{H}_h : \mathbf{Z}_h \tag{3.3}$$

for all tensor-valued test fields $\boldsymbol{Z}_h \in S_h^{3\times 3}(\Gamma_h)$.

Remark 3.6. The version (3.3) for the shape operator employed by us stems from [27] and was shown in [28] to satisfy

$$\|\widetilde{\mathbf{Q}}_h - \nabla_\Gamma \boldsymbol{\nu}\|_{L^2(\Gamma)} = O(h)$$

(where $\widetilde{\mathbf{Q}}_h$ is an appropriate lift of Q_h from Γ_h to Γ, see [28] for the details) provided that the sufficiently smooth limiting surface Γ is interpolated by the triangulated surfaces Γ_h, i.e., vertices and edge-midpoints are projected to Γ. Furthermore, numerical experiments indicate that this convergence also holds true in $L^\infty(\Gamma)$. We remark that for such convergence results we need quadratic finite elements and linear finite elements are not sufficient. Another possibility for approximating the shape operator is to compute $\nabla_{\Gamma_h}\boldsymbol{\nu}_h$ on (more precisely, in the interior of) every $T \in \mathcal{T}_h$. As shown in [14] this converges to $\nabla_\Gamma \nu$ in L^2 and L^∞ linearly in h for quadratic (but not for linear) elements where again Γ is the known smooth limit of the surfaces Γ_h obtained by interpolation.

3.2. Discrete problems

3.2.1. Discretization in space

For dynamic problems we will consider families of triangulated surfaces $\{\Gamma_h(t)\}_{t\in I}$ where each $\Gamma_h(t)$ has the above properties and the nodes $\boldsymbol{x}_i(t)$ depend smoothly on the relaxation time t. The velocity

$$\boldsymbol{\nu}_h(t,\boldsymbol{x}) := \sum_i \partial_t \boldsymbol{x}_i(t)\phi_i(t,\boldsymbol{x}) \tag{3.4}$$

is an element of $\boldsymbol{S}_h(\Gamma_h(t))$ and is tacitly taken into account in the operator $\partial_t^\bullet$ whenever working on a triangulated surface. We remark that (see [19])

$$\partial_t^\bullet \phi_i = (\partial_t + \boldsymbol{\nu}_h \cdot \nabla)\phi_i = 0 \quad \forall i = 1,\dots,N_h. \tag{3.5}$$

Also the other t-dependent surface fields will become families of finite element functions as, e.g., $\{\boldsymbol{H}_h(t)\}_t$ where the t dependence concerns the coefficient vector $\underline{\boldsymbol{H}}(t)$ but also the basis functions $\boldsymbol{e}_k\phi_i(t,\cdot)$ of $\boldsymbol{S}_h(\Gamma_h(t))$.

Definition 3.7. Let $\{\Gamma_h(t), c(t)\}_{t\in I}$ be an evolving discrete admissible phase field surface for which $H_h(t)$ and $Q_h(t)$ denote the discrete mean curvature vector and Weingarten map equation at each $t \in I$, respectively. Further, let $(\lambda_V^h, \lambda_A^h, \lambda_c^h) : I \to \mathbb{R}^3$. The following variational equations are defined at each time $t \in I$.

The *discrete variational surface equation* reads

$$\begin{aligned}\mathcal{L}(\Gamma_h; \boldsymbol{\nu}_h, \boldsymbol{w}_h) = &-\mathcal{W}(\Gamma_h; \boldsymbol{H}_h, \boldsymbol{w}_h) - \mathcal{G}_1(\Gamma_h; c_h, \mathbf{Q}_h, \boldsymbol{w}_h) - \mathcal{G}_2(\Gamma_h; c_h, \boldsymbol{H}_h, \boldsymbol{w}_h) - \mathcal{M}_1(\Gamma_h; \boldsymbol{H}_h)\mathcal{M}_2(\Gamma_h; \mathbf{Q}_h, \boldsymbol{w}_h)\\ &- \lambda_V^h \mathcal{N}(\Gamma_h; \boldsymbol{w}_h) - \lambda_A^h \mathcal{L}(\Gamma_h; \boldsymbol{H}_h, \boldsymbol{w}_h) - \lambda_c^h \mathcal{L}(\Gamma_h; h(c_h)\boldsymbol{H}_h, \boldsymbol{w}_h)\end{aligned} \tag{3.6}$$

for a test vector field $w_h \in S_h(\Gamma_h)$.

The *discrete variational phase field equation* is defined by

$$\omega\varepsilon\mathcal{L}_s(\Gamma_h; \partial_t^\bullet c_h, \phi_h) = -\varepsilon\sigma\mathcal{E}_s(\Gamma_h; c_h, \phi_h) - \frac{\sigma}{\varepsilon}\mathcal{L}_s(\Gamma_h; W'(c_h), \phi_h) - \lambda_c^h \mathcal{L}_s(\Gamma_h; h'(c_h), \phi_h) \tag{3.7}$$

for a scalar test function $\phi_h \in S_h(\Gamma_h)$.

The *discrete constraint equations* are

$$0 = \mathcal{C}_V^h(\Gamma_h) = \frac{1}{3}\mathcal{N}(\Gamma_h; \boldsymbol{x}_h) - V, \tag{3.8}$$

$$0 = \mathcal{C}_A^h(\Gamma_h) = \frac{1}{2}\mathcal{E}(\Gamma_h; \boldsymbol{x}_h, \boldsymbol{x}_h) - (A_1 + A_2), \tag{3.9}$$

$$0 = \mathcal{C}_c^h(\Gamma_h, c_h) = \mathcal{L}_s(\Gamma_h; h(c_h), 1) - (A_1 - A_2). \tag{3.10}$$

Remark 3.8. In the above recall that the velocity has the nodal values $v_{i,k}(t) = \partial_t x_{i,k}(t)$, and by the transport property of the basis functions (3.5) we see that

$$\partial_t^\bullet c_h = \sum_i \partial_t^\bullet (c_i\phi_i) = \sum_i \partial_t^\bullet c_i \phi_i + c_i \partial_t^\bullet \phi_i = \sum_i \partial_t c_i \phi_i.$$

Please cite this article in press as: C.M. Elliott, B. Stinner, Modeling and computation of two phase geometric biomembranes using surface finite elements, J. Comput. Phys. (2010), doi:10.1016/j.jcp.2010.05.014

Remark 3.9. Deforming Γ_h by a field $w_h \in S_h(\Gamma_h)$ yields quadratic triangulated surfaces again. Variations of the constraints (3.8) and (3.9) based on such deformations read similar as in the continuous setting (see Lemma 2.7):

$$\langle \delta \mathcal{C}_V^h(\Gamma_h), \boldsymbol{w}_h \rangle = \mathcal{N}(\Gamma_h; \boldsymbol{w}_h), \tag{3.11}$$

$$\langle \delta \mathcal{C}_A^h(\Gamma_h), \boldsymbol{w}_h \rangle = \mathcal{E}(\Gamma_h; \boldsymbol{x}_h, \boldsymbol{w}_h) = \mathcal{L}(\Gamma_h; \boldsymbol{H}_h, \boldsymbol{w}_h). \tag{3.12}$$

Problem 3.10 (*Semi-discrete variational relaxation flow*). Suppose that data $\{V, A_1, A_2\}$ fulfilling (2.1) and a discrete admissible phase field surface (Γ_h^0, c_h^0) are given such that

$$V = |\Omega_h^0|, \quad A_1 + A_2 = |\Gamma_h^0|, \quad A_1 - A_2 = \mathcal{L}_s(\Gamma_h; h(c_h^0), 1). \tag{3.13}$$

Find a family of discrete admissible phase field surfaces $\{(\Gamma_h(t), c(t))\}_{t\in I}$ with $(\Gamma_h(0), c_h(0)) := (\Gamma_h^0, c_h^0)$ and find functions $\lambda_{V,h}, \lambda_{A,h}, \lambda_{c,h} : [0,\infty) \to \mathbb{R}$ such that the discrete surface, phase field and constraint Eqs. (3.6)–(3.10) are fulfilled at each time $t \in I$ where the fields $\{H_h(t)\}_t$ and $\{Q_h(t)\}_t$ are computed from (3.2) and (3.3), respectively.

3.2.2. Full discretization

In order to discretize in time we consider times $\{t^m\}_{m\in\mathbb{N}}$ with $t^m \in [0,\infty)$, $t^m > t^{m-1}$, and $t^m \to \infty$ as $m \to \infty$ and set $\tau^m := t^{m+1} - t^m$ for the time steps. Quantities at time t^m are denoted with an upper index m. At any time level m the surface Γ_h^m is given by knowledge of $\boldsymbol{x}_h^m$, the vertices of the triangulation. On each surface Γ_h^m we define the fields $\widetilde{\boldsymbol{H}}_h^m \in \boldsymbol{S}_h(\Gamma_h^m)$ and $\boldsymbol{Q}_h^m \in S_h^{3\times 3}(\Gamma_h^m)$ by (3.2) and (3.3), respectively, i.e.

$$\mathcal{L}(\Gamma_h^m; \widetilde{\boldsymbol{H}}_h^m, \boldsymbol{w}_h) = \mathcal{E}(\Gamma_h^m; \boldsymbol{x}_h^m, \boldsymbol{w}_h) \tag{3.14}$$

for all $\boldsymbol{w}_h \in \boldsymbol{S}_h(\Gamma_h^m)$ and

$$\int_{\Gamma_h^m} \boldsymbol{Q}_h^m : \boldsymbol{Z}_h = \int_{\Gamma_h^m} \left(-(\nabla_{\Gamma_h} \cdot \boldsymbol{Z}_h) \cdot \boldsymbol{v}_h^m + \boldsymbol{v}_h^m \otimes \widetilde{\boldsymbol{H}}_h^m : \boldsymbol{Z}_h \right) \tag{3.15}$$

for all tensor-valued test fields $\boldsymbol{Z}_h \in S_h^{3\times 3}(\Gamma_h)$. For notational convenience we set (for $\boldsymbol{w}_h \in \boldsymbol{S}_h(\Gamma_h^m)$)

$$\begin{aligned} \mathcal{Z}^m(\boldsymbol{w}_h) = &-k_H \mathcal{R}(\Gamma_h^m; \widetilde{\boldsymbol{H}}_h^m, \boldsymbol{w}_h) - k_H \mathcal{D}(\Gamma_h; \widetilde{\boldsymbol{H}}_h^m, \boldsymbol{w}_h) - \mathcal{G}_1\left(\Gamma_h^m; c_h^m, \boldsymbol{Q}_h^m, \boldsymbol{w}_h\right) - \mathcal{G}_2(\Gamma_h^m; c_h^m, \widetilde{\boldsymbol{H}}_h^m, \boldsymbol{w}_h) \\ &- \mathcal{M}_1(\Gamma_h^m; \widetilde{\boldsymbol{H}}_h^m) \mathcal{M}_2(\Gamma_h^m; \boldsymbol{v}_h^m, \boldsymbol{Q}_h^m, \boldsymbol{w}_h) - \lambda_c^{h,m} \mathcal{L}(\Gamma_h^m; h(c_h^m) \widetilde{\boldsymbol{H}}_h^m, \boldsymbol{w}_h). \end{aligned} \tag{3.16}$$

To step from a time level to the next one we decouple the computation of the surface from that of the order parameter.

Definition 3.11 (*Fully discrete scheme*). Assume that an initial discrete admissible phase field surface (Γ_h^0, c_h^0) is given such that (3.13) holds for data $\{V, A_1, A_2\}$ fulfilling (2.1). Set $\lambda_{c,h}^0 = 0$. The *fully discrete scheme* consists of computing discrete admissible phase field surfaces (Γ_h^m, c_h^m) subsequently for $m = 0, 1, 2, \ldots$ as follows:

1. **Fully discrete evolution of the surface:** Given a discrete admissible phase field surface (Γ_h^m, c_h^m) at time t^m, the field $\boldsymbol{x}_h^{m+1} \in \boldsymbol{S}_h(\Gamma_h^m)$ defining the surface Γ_h^{m+1}, the discrete mean curvature vector $\boldsymbol{H}_h^{m+1} \in \boldsymbol{S}_h(\Gamma_h^m)$ and the Lagrange multipliers $\lambda_V^{h,m+1}$ and $\lambda_A^{h,m+1}$ at time t^{m+1} are obtained from the equations

$$\mathcal{L}\left(\Gamma_h^m; \frac{\boldsymbol{x}_h^{m+1} - \boldsymbol{x}_h^m}{\tau^m}, \boldsymbol{w}_h\right) + k_H \mathcal{E}(\Gamma_h^m; \boldsymbol{H}_h^{m+1}, \boldsymbol{w}_h) + \lambda_V^{h,m+1} \mathcal{N}(\Gamma_h^m; \boldsymbol{w}_h) + \lambda_A^{h,m+1} \mathcal{L}(\Gamma_h^m; \widetilde{\boldsymbol{H}}_h^m, \boldsymbol{w}_h) = \mathcal{Z}^m(\boldsymbol{w}_h), \tag{3.17}$$

$$\mathcal{L}(\Gamma_h^m; \boldsymbol{H}_h^{m+1}, \zeta_h) - \mathcal{E}(\Gamma_h^m; \boldsymbol{x}_h^{m+1}, \zeta_h) = 0, \tag{3.18}$$

$$\mathcal{C}_V^h(\Gamma_h^{m+1}) = 0, \tag{3.19}$$

$$\mathcal{C}_A^h(\Gamma_h^{m+1}) = 0, \tag{3.20}$$

where (3.17) and (3.18) have to hold for all vector fields $\boldsymbol{w}_h, \zeta_h \in \boldsymbol{S}_h(\Gamma_h^m)$.

2. **Fully discrete evolution of the phase field:** Given a discrete admissible phase field surface (Γ_h^m, c_h^m) at time t^m and a surface Γ_h^{m+1} at time t^{m+1} the field $c_h^{m+1} \in S_h(\Gamma_h^m)$ and the Lagrange multiplier $\lambda_c^{h,m+1}$ are obtained from

$$\omega\varepsilon \mathcal{L}_s\left(\Gamma_h^{m+1}; \frac{c_h^{m+1} - \tilde{c}_h^m}{\tau^m}, \phi_h\right) + \varepsilon\sigma \mathcal{E}_s(\Gamma_h^{m+1}; c_h^{m+1}, \phi_h) + \lambda_c^{h,m+1} \mathcal{L}_s(\Gamma_h^{m+1}; h'(c_h^m), \phi_h) = \frac{\sigma}{\varepsilon} \mathcal{L}_s(\Gamma_h^{m+1}; W'(c_h^m), \phi_h), \tag{3.21}$$

$$\mathcal{C}_c^h(\Gamma_h^{m+1}, c_h^{m+1}) = 0, \tag{3.22}$$

where (3.21) has to hold for all $\phi_h \in S_h(\Gamma_h^{m+1})$ and where $\tilde{c}_h^m \in S_h(\Gamma_h^{m+1})$ is defined by $\tilde{c}_h^m(\boldsymbol{x}) = \sum_{i=1}^{N_h} c_i^m \phi_i^{m+1}(\boldsymbol{x})$.

Please cite this article in press as: C.M. Elliott, B. Stinner, Modeling and computation of two phase geometric biomembranes using surface finite elements, J. Comput. Phys. (2010), doi:10.1016/j.jcp.2010.05.014

3.3. Solution algorithm

Let us denote the mass and the stiffness matrix by

$$M := (M_{ij})_{i,j=1}^{N_h}, M_{ij} := \int_{\Gamma_h} \phi_i \phi_j, \quad A := (A_{ij})_{i,j=1}^{N_h}, \quad A_{ij} := \int_{\Gamma_h} \nabla_{\Gamma_h} \phi_i \cdot \nabla_{\Gamma_h} \phi_j$$

and their 3×3 block versions by $\boldsymbol{M} = (\delta_{kl} M)_{k,l=1}^3$ and $\boldsymbol{A} = (\delta_{kl} A)_{k,l=1}^3$.

3.3.1. Iterative procedure for the surface

The surface update step consisting of (3.17) and (3.18) from time level m to $m+1$ in Scheme 3.11 may be written in matrix–vector form as

$$\begin{pmatrix} \frac{1}{\tau^m}\boldsymbol{M}^m & k_H \boldsymbol{A}^m \\ -\boldsymbol{A}^m & \boldsymbol{M}^m \end{pmatrix} \begin{pmatrix} \underline{\boldsymbol{x}}^{m+1} \\ \underline{\boldsymbol{H}}^{m+1} \end{pmatrix} = \begin{pmatrix} \frac{1}{\tau^m}\boldsymbol{M}^m \underline{\boldsymbol{x}}^m + \underline{\boldsymbol{z}}^m \\ 0 \end{pmatrix} - \lambda_{V,h}^{m+1} \begin{pmatrix} \underline{\boldsymbol{n}}^m \\ 0 \end{pmatrix} - \lambda_{A,h}^{m+1} \begin{pmatrix} \underline{\boldsymbol{k}}^m \\ 0 \end{pmatrix}$$

where

$$\begin{aligned} &\boldsymbol{z}_h^m \in \boldsymbol{S}_h(\Gamma_h^m), \quad \boldsymbol{z}_{i,k} = \mathcal{Z}^m(\boldsymbol{e}_k \phi_i), \\ &\boldsymbol{n}_h^m \in \boldsymbol{S}_h(\Gamma_h^m), \quad \boldsymbol{n}_{i,k} = \mathcal{N}(\Gamma_h^m; \boldsymbol{e}_k \phi_i), \\ &\boldsymbol{k}_h^m \in \boldsymbol{S}_h(\Gamma_h^m), \quad \boldsymbol{k}_{i,k} = \mathcal{L}(\Gamma_h^m; \widetilde{\boldsymbol{H}}_h^m, \boldsymbol{e}_k \phi_i) \overset{(3.14)}{=} \mathcal{E}(\Gamma_h^m; \boldsymbol{x}_h^m, \boldsymbol{e}_k \phi_i). \end{aligned} \tag{3.23}$$

Thus setting

$$\boldsymbol{I}^m := \begin{pmatrix} \frac{1}{\tau^m}\boldsymbol{M}^m & k_H \boldsymbol{A}^m \\ -\boldsymbol{A}^m & \boldsymbol{M}^m \end{pmatrix}$$

and then defining

$$(\boldsymbol{I}^m)^{-1} \begin{pmatrix} \underline{\boldsymbol{n}}^m \\ 0 \end{pmatrix} =: \boldsymbol{q}^m = \begin{pmatrix} \underline{\boldsymbol{q}}_1^m \\ \underline{\boldsymbol{q}}_2^m \end{pmatrix}, \quad (\boldsymbol{I}^m)^{-1} \begin{pmatrix} \underline{\boldsymbol{k}}^m \\ 0 \end{pmatrix} =: \boldsymbol{s}^m = \begin{pmatrix} \underline{\boldsymbol{s}}_1^m \\ \underline{\boldsymbol{s}}_2^m \end{pmatrix}.$$

we have

$$\begin{pmatrix} \underline{\boldsymbol{x}}^{m+1} \\ \underline{\boldsymbol{H}}^{m+1} \end{pmatrix} = (\boldsymbol{I}^m)^{-1} \begin{pmatrix} \frac{1}{\tau^m}\boldsymbol{M}^m \underline{\boldsymbol{x}}^m + \underline{\boldsymbol{r}}^m \\ 0 \end{pmatrix} - \lambda_V^{h,m+1} \boldsymbol{q}^m - \lambda_A^{h,m+1} \boldsymbol{s}^m. \tag{3.24}$$

In view of the constraints (3.19) and (3.20) we may write

$$0 = f(\lambda^{m+1}) := \begin{pmatrix} \mathcal{C}_V^h(\Gamma_h^{m+1}(\lambda^{m+1})) \\ \mathcal{C}_A^h(\Gamma_h^{m+1}(\lambda^{m+1})) \end{pmatrix}$$

where $\lambda^{m+1} = (\lambda_V^{h,m+1}, \lambda_A^{h,m+1})$. This is solved by a Newton method for which we need the derivative of f. We see from (3.24) that a change in $\lambda_V^{h,m+1}$ corresponds to a deformation of $\Gamma_h^{m+1}(\lambda)$ in the direction $-\boldsymbol{q}_{1,h}^m$ which is the finite element function associated with the vector $-\underline{\boldsymbol{q}}_1^m$. The partial derivative of f with respect to $\lambda_V^{h,m+1}$ therefore corresponds to the variation of $\mathcal{C}_V^h$ and $\mathcal{C}_A^h$ in direction $-\boldsymbol{q}_h^m$. The treatment of the derivatives with respect to $\lambda_A^{h,m+1}$ is similar. In view of the formulae (3.11), (3.12) and the definitions of $\underline{\boldsymbol{n}}$ and $\underline{\boldsymbol{k}}$ we obtain

$$Df(\lambda^{m+1}) = \begin{pmatrix} \partial_{\lambda_V} \mathcal{C}_V^h(\Gamma_h^{m+1}(\lambda^{m+1})) & \partial_{\lambda_A} \mathcal{C}_V^h(\Gamma_h^{m+1}(\lambda^{m+1})) \\ \partial_{\lambda_V} \mathcal{C}_A^h(\Gamma_h^{m+1}(\lambda^{m+1})) & \partial_{\lambda_A} \mathcal{C}_A^h(\Gamma_h^{m+1}(\lambda^{m+1})) \end{pmatrix} = -\begin{pmatrix} \underline{\boldsymbol{n}}^{m+1} \cdot \underline{\boldsymbol{q}}_1^m & \underline{\boldsymbol{n}}^{m+1} \cdot \underline{\boldsymbol{s}}_1^m \\ \underline{\boldsymbol{k}}^{m+1} \cdot \underline{\boldsymbol{q}}_1^m & \underline{\boldsymbol{k}}^{m+1} \cdot \underline{\boldsymbol{s}}_1^m \end{pmatrix}.$$

We perform an iteration of the form

$$\lambda^{m+1,k+1} = \lambda^{m+1,k} - (Df(\lambda^{m+1,k}))^{-1} f(\lambda^{m+1,k}) \tag{3.25}$$

to compute the values λ^{m+1}. The values $\lambda^{m+1,0} = \lambda^m$, $\lambda^{0,0} = 0$ are taken as initial choice. The iteration is stopped if the values $\mathcal{C}_V(\Gamma^{m+1}(\lambda^{m+1,k+1}))/V$ and $\mathcal{C}_A(\Gamma^{m+1}(\lambda^{m+1,k+1}))/(A_1 + A_2)$ are reduced below a given tolerance. In our simulations we chose 10^{-12} as tolerance and observed that usually only a few Newton iteration steps were necessary to achieve the desired accuracy. Damping has never been required to ensure convergence.

3.3.2. Iterative procedure for the phase field

With respect to the phase separation update step from time level m to $m+1$ in the Scheme 3.11 we observe that Eq. (3.21) may be written in the form

$$R^{m+1} \underline{c}^{m+1} = \frac{\varepsilon\omega}{\tau^m} M^{m+1} \underline{c}^m - \underline{w}^{m+1,m} - \lambda_{c,h}^{m+1} \underline{p}^{m+1,m},$$

Please cite this article in press as: C.M. Elliott, B. Stinner, Modeling and computation of two phase geometric biomembranes using surface finite elements, J. Comput. Phys. (2010), doi:10.1016/j.jcp.2010.05.014

where $R^{m+1} := \frac{\varepsilon\omega}{\tau^m} M^{m+1} + \varepsilon\sigma A^{m+1}$ and where the fields

$$w_h^{m+1,m} \in S_h(\Gamma_h^{m+1}), \quad w_i = \frac{\sigma}{\varepsilon}\mathcal{L}_s(\Gamma_h^{m+1}; W'(c_h^m), \phi_i),$$
$$p_h^{m+1,m} \in S_h(\Gamma_h^{m+1}), \quad p_i = \mathcal{L}_s(\Gamma_h^{m+1}; h'(c_h^m), \phi_i)$$

are used.

Again we apply the Newton method to compute the Lagrange multiplier $\lambda_{c,h}^{m+1}$ so that the constraint (3.22) is satisfied at time t^{m+1}. The procedure is similar to the one described above and a detailed description therefore is omitted.

3.3.3. Algorithm

The proposed algorithm to compute the new membrane Γ_h^{m+1} from Γ_h^m consists of (i) successively solving three linear systems for the matrix $\boldsymbol{I}^m$ (recall (3.24)), performing the Newton iteration (3.25) which involves computing the new surface Γ_h^{m+1} and new curvature $\boldsymbol{H}_h^{m+1}$, (iii) solve the two linear systems $(R^{m+1})^{-1}\underline{w}^{m+1,m}$ and $(R^{m+1})^{-1}\underline{p}^{m+1,m}$ for the phase separation equation, and (iv) perform the Newton iteration for the Lagrange multiplier $\lambda_{c,h}^{m+1}$ which involves computing the new order parameter c_h^{m+1}.

The overall procedure as described above is summarized in Algorithm 1. Issues like stopping criteria and choice of the time step are discussed in the section on the numerical simulations.

Algorithm 1. Membrane evolution with phase separation

input: Initial discrete admissible phase field surface (Γ_h^0, c_h^0),
output: Relaxed discrete admissible phase field surface $(\Gamma_h^{\bar m}, c_h^{\bar m})$ and discrete mean curvature vector $\boldsymbol{H}_h^{\bar m}$ at some (sufficiently large) time $t^{\bar m} > 0$,
assemble M^0 and A^0 and its 3×3 diagonal block versions,
factories M^0,
for $m = 0, \dots, \bar m - 1$ **do**
  adapt the grid based on the given data and choose a time step τ^m,
  assemble $\underline{\boldsymbol{r}}^m, \underline{\boldsymbol{n}}^m, \underline{\boldsymbol{k}}^m, \boldsymbol{I}^m$,
  solve $(\boldsymbol{I}^m)^{-1}(\frac{1}{\tau^m}M^m\underline{\boldsymbol{x}}^m + \underline{\boldsymbol{z}}^m, 0)^T$, $(\boldsymbol{I}^m)^{-1}(\underline{\boldsymbol{n}}^m, 0)^T$, and $(\boldsymbol{I}^m)^{-1}(\underline{\boldsymbol{k}}^m, 0)^T$,
  perform a Newton iteration for the Lagrange multipliers $\lambda_{V,h}^{m+1}, \lambda_{A,h}^{m+1}$ and compute $\underline{\boldsymbol{x}}^{m+1}, \underline{\boldsymbol{H}}^{m+1}$,
  assemble $\underline{w}^{m+1,m}, \underline{p}^{m+1,m}, R^{m+1}, M^{m+1}$
  solve $(R^{m+1})^{-1}\left(\frac{\varepsilon}{\tau^m}M^{m+1}\underline{c}^m - \underline{w}^{m+1,m}\right)$ and $(R^{m+1})^{-1}\underline{p}^{m+1,m}$,
  perform a Newton iteration for the Lagrange multiplier $\lambda_{c,h}^{m+1}$ and compute $\underline{c}^{m+1}$,
end for

Remark 3.12. The main computational cost in our simulations arose from solving the linear systems. Taking explicit choices for the Lagrange multipliers would involve only two linear systems for $(\underline{x}^{m+1}, \underline{H}^{m+1})$ and $\underline{c}^{m+1}$ (which could be written as one big systems, of course). But for the system sizes in our simulations direct methods for factorizing the matrices were suitable so that the cost for solving multiple systems instead of only two is small. Furthermore, by reordering the unknowns by the coordinates, i.e. in the form

$$(\underline{\boldsymbol{x}}, \underline{\boldsymbol{H}})^{m+1} \to (\boldsymbol{x}_{1,1}, \dots, \boldsymbol{x}_{N_h,1}, \boldsymbol{H}_{1,1}, \dots, \boldsymbol{H}_{N_h,1}, \boldsymbol{x}_{1,2}, \dots, \boldsymbol{H}_{N_h,2}, \boldsymbol{x}_{1,3}, \dots, \boldsymbol{H}_{N_h,3})^{m+1}$$

the matrix I^m involves diagonal blocks of the form

$$\begin{pmatrix} \frac{1}{\tau^m}M^m & k_H A^m \\ -A^m & M^m \end{pmatrix},$$

and the off-diagonal blocks are zero, whence it is sufficient to factorize these blocks which are of size $2N_h$. Setting $\sigma = 0$, $\alpha = 0$ and $k_H = 1$ we end up having this property for Willmore flow. For comparison, the system size of the method in [2] for Willmore flow is $4N_h$. In [18], where our method for the bending energy stems from, more terms contained in $\mathcal{R}$ are taken into account semi-implicitly in time, and as a consequence the off-diagonal blocks do not vanish any more so that a system of size $6N_h$ has to be solved in each time step.

Remark 3.13. When replacing $\widetilde{\boldsymbol{H}}_h^m$ in (3.16) and, hence, in (3.23) by $\boldsymbol{H}_h^m$ we observed that the grid quality was gently worse which motivates the choice of $\widetilde{\boldsymbol{H}}_h$ there. Moreover, we then need no initial values for the curvature. Towards the end of the relaxation the nodes essentially do not move any more so that the new curvature field $\boldsymbol{H}_h^{m+1}$ practically coincides with $\widetilde{\boldsymbol{H}}_h^{m+1}$.

Please cite this article in press as: C.M. Elliott, B. Stinner, Modeling and computation of two phase geometric biomembranes using surface finite elements, J. Comput. Phys. (2010), doi:10.1016/j.jcp.2010.05.014

Remark 3.14. Taking the term from the double-well potential and the mass constraint explicitly in time in the Allen–Cahn equation, i.e., $\underline{w}^{m+1,m}$ instead of $\underline{w}^{m+1,m+1}$, leads to a mild stability restriction on the time step of the form $\tau \lesssim \varepsilon^2/\omega$. In the simulations presented below we chose $\tau \sim h^2$ and always had $h \lesssim \varepsilon$ whenever computing problems involving a phase separation. Stability problems never occurred.

3.3.4. Adaptive local grid refinement

Algorithm 2. Marking Strategy for adaptive refinement

input: Triangulated surface Γ_h with order parameter c_h and curvature vector $\boldsymbol{H}_h$ and marking strategy (N_{in}, N_{off}, N_H),
output: A number $f(T) \in \{-1,0,1\}$ for each element $T \in \mathcal{T}_h$ indicating whether T has to be refined ($f(T) = 1$) or may be coarsened ($f(T) = -1$),
for $T \in \mathcal{T}_h$ **do**
compute the diameter diam (T) of T,
find the maximal value I_c of $|c_h|$ in the six nodes,
compute I_H as the mean of the values of $\sqrt{s_{H,h}}$ in the six nodes of T,
set $f(T) = 0$,
if $I_c < 0.97$ (i.e., if we are within the interfacial layer) **then**
if diam $(T) > \varepsilon/N_{in}$ or diam $(T) > N_H/I_H$ **then**
set $f(T) = 1$,
else if diam $(T) < \varepsilon/(2N_{in})$ and diam $(T) < N_H/(2I_H)$ **then**
set $f(T) = -1$,
end if
else
(i.e., we are in the pure phase)
if diam $(T) > \varepsilon/N_{off}$ or diam $(T) > N_H/I_H$ **then**
set $f(T) = 1$,
else if diam $(T) < \varepsilon/(2N_{off})$ and diam $(T) < N_H/(2I_H)$ **then**
set $f(T) = -1$.
end if
end if
end for

As the interfacial thickness parameter ε becomes small it is desirable to adaptively refine the grid, mainly in the transition regions of the order parameter but also in strongly curved regions. The finite element software ALBERTA [35] that we used for implementing our scheme requires a marking function that provides a flag for each element indicating whether it has to be refined (=bisected) or whether it may be coarsened. We want to ensure that the interfacial layers are resolved by the mesh but also demand the strongly curved regions to contain sufficient numbers of nodes. For the latter ones we consider the quantity

$$s_H := |\nabla_\Gamma \boldsymbol{\nu}|^2 = H_1^2 + H_2^2 = H^2 - 2K,$$

i.e., the sum of the squares of the principal curvatures. The Gaussian curvature can be computed via

$$K = \det(\boldsymbol{I} + \nabla_\Gamma \boldsymbol{\nu}) - H - 1,$$

and as discussed in [28] the discrete analog

$$K_h(\boldsymbol{x}) = \sum_{i=1}^{N_h} K_i \phi_i(\boldsymbol{x}), \quad K_i = \det(\boldsymbol{I} + \boldsymbol{Q}_h) - \operatorname{trace}(\boldsymbol{Q}_h) - 1,$$

is a good approximation. Hence, we define the discrete version of s_H by

$$s_{H,h}(\boldsymbol{x}) = \sum_{i=1}^{N_h} s_{H,i} \phi_i(\boldsymbol{x}), \quad s_{H,i} = |\boldsymbol{H}_i|^2 - 2K_i.$$

Our *marking strategy* consists of three positive numbers (N_{in}, N_{off}, N_H) with the following meaning: The diameter of an element in the interfacial layer shall be smaller than ε/N_{in}, and if the element belongs to one of the bulk phases then the diameter shall be smaller than ε/N_{off}, and throughout the element diameter shall be smaller than N_H/I_H where I_H is the arithmetic mean of the values of $\sqrt{s_{H,h}}$ in the nodes belonging to the element. Algorithm 2 carefully states when triangles are marked for refinement or coarsening.

Remark 3.15. Clearly one could also have taken $s_{H,i} = |(Q_h)_i|^2$ as an approximation to the sum of the squares of the principal curvature. We have not tried out other approaches since the refinement should be part of procedures to keep a good mesh

Please cite this article in press as: C.M. Elliott, B. Stinner, Modeling and computation of two phase geometric biomembranes using surface finite elements, J. Comput. Phys. (2010), doi:10.1016/j.jcp.2010.05.014

property even in the case of large deformations. We leave a careful analysis of this issue and of improving the efficiency of the above method for future research but note that applying it makes the computations significantly cheaper.

We performed an explicit mesh adaption strategy and executed the marking algorithm at the beginning of every third time step followed by the mesh adaption. During the latter one the fields on the surface are interpolated and restricted to obtain the values in the new nodes as described in [35]. Often, this leads to an increase of the total energy and, in particular, the surface data are no longer consistent in the following sense: For a triangulated surface in (or close to) equilibrium Eq. (3.2) is fulfilled and relates $\boldsymbol{x}_h$ and $\boldsymbol{H}_h$, and mesh adaptivity typically destroys this relation. But we observed that the system quickly relaxes back and decreases the energy to the previous state. For this reason we perform a couple of time steps before considering another mesh adaptation. We also observed that in the late stage of the simulation when the system has almost relaxed mesh changes are no longer needed.

4. Numerical experiments

We first look at the pure Helfrich flow (no phase separation) before discussing convergence in h and ε in Section 4.3. In subsequent sections we investigate the consistency of our results with the phase diagram for axisymmetric shapes (Section 4.5), effects due to the area-difference term $\mathcal{F}_M$ in (1.2), we study non axisymmetric two-phase membranes (Section 4.7) and a situation that can involve a topological change of the phases (Section 4.8).

4.1. Monitored quantities

To measure the discrete energy we compute

$$\mathcal{F}_h = \mathcal{F}_W^h + \mathcal{F}_{GL}^h + \mathcal{F}_M^h = k_H \int_{\Gamma_h} \frac{1}{2}|\boldsymbol{H}_h|^2 + \sigma \int_{\Gamma_h} \left(\frac{\varepsilon}{2}|\nabla_{\Gamma_h} c_h|^2 + \frac{1}{\varepsilon} W(c_h)\right) + \frac{k_H \alpha}{8}\left(\frac{1}{\overline{R}}\int_{\Gamma_h} \boldsymbol{H}_h \cdot \boldsymbol{\nu}_h - m_0\right)^2.$$

Since the surface mesh is evolving we monitored the mesh quality. As one quality measure $q(\Gamma_h)$ of the polyhedral surface Γ_h we have used the minimal value of the sinus of the interior angles of the elements,

$$q(\Gamma_h) := \min\{q_T | T \in \mathcal{T}(\Gamma_h)\}, \quad q_T := \min\{\sin(\alpha) | \alpha \text{ inner angle of } T\}. \tag{4.1}$$

With inner angles we mean all angles of the four flat triangles formed by neighboring nodes: Recalling that any $T \in \mathcal{T}_h$ has six nodes, three of them corresponding to the vertices and three located on the edges, we consider the three planar triangles formed by a vertex and the nodes on the adjacent edges and the triangle formed by the nodes on the edges.

Whenever we refer to the velocity field we mean the finite element function

$$\boldsymbol{v}_h^m \in \boldsymbol{S}_h(\Gamma_h^m), \quad \boldsymbol{v}_{i,k}^m := \frac{\boldsymbol{x}_{i,k}^m - \boldsymbol{x}_{i,k}^{m-1}}{\tau^{m-1}}.$$

The numerical error of convergence has been measured in the form

$$eoc(\mathcal{F}_h) := \frac{\log(|\mathcal{F}_h(\sqrt{2}\varepsilon) - \mathcal{F}_h(\varepsilon)|/|\mathcal{F}_h(\varepsilon) - \mathcal{F}_h(\varepsilon/\sqrt{2})|)}{\log(\sqrt{2})} \tag{4.2}$$

and analogously for $\lambda_{V,h}$ and $\lambda_{c,h}$.

Unless otherwise stated the time step has always been chosen to be $\tau^m \lesssim (h_{min}^0)^2$ where h_{min}^0 is the initial minimal edge length.

4.2. Helfrich flow

We first report on some consistency tests for elastic membranes without lateral phase separation, i.e. we set $c \equiv 1$. The gradient flow dynamics of the bending energy subject to constraints on area and volume but no area difference term ($\alpha = 0$) is commonly known as Helfrich flow. We relaxed some appropriate initial shapes and compared the energies in the relaxed states with results from [38] where phase diagrams for various models of axisymmetric lipid bilayer vesicles have been derived.

The scale invariance of the bending energy is an important issue since it reduces the number of effective parameters on which the energetically most favorable state depends: Under a dilation of the space the energy $\mathcal{F}_W(\Gamma)$ does not change. We recall that the quantity

$$\overline{R} = \sqrt{A/4\pi}$$

had been introduced as a reference length scale and is the radius of the sphere with surface area $A := A_1 + A_2$. Equilibrium shapes effectively only depend on the reduced volume

Please cite this article in press as: C.M. Elliott, B. Stinner, Modeling and computation of two phase geometric biomembranes using surface finite elements, J. Comput. Phys. (2010), doi:10.1016/j.jcp.2010.05.014

$$\overline{V} := V/\left(\frac{4}{3}\pi\overline{R}^3\right).$$

We remark that if Γ topologically is a sphere then $\overline{V} \in [0,1]$ because the sphere minimizes the surface area among all surfaces of that topological type enclosing a given volume.

We employed an adaptive time stepping by setting

$$\tau^m = \frac{(h^0_{min})^2}{10\overline{R}\max\limits_i |\boldsymbol{v}^{m-1}_{i,\cdot}|}$$

where $\max_{i\in N_h}|\boldsymbol{v}_{i,\cdot}|$ is the maximal node velocity, h^0_{min} is the initial minimal edge length, and the length scale $\overline{R}$ is taken into account for scale invariance. We remark that taking the minimal edge length at time t^m instead of h^0_{min} into account did not essentially change the results of our simulations. The simulations were terminated when the maximal node velocity was small enough, namely when

$$\max_{i\in N_h}|\boldsymbol{v}_{i,\cdot}| \leqslant \overline{R}\times 10^{-4}.$$

The initial shapes and the data for the relaxed shapes are listed in Table 1. For $\overline{V}\approx 0.62$ the discocyte shape has less energy than the dumbbell shape whilst for $\overline{V}\approx 0.79$ the situation is vice versa. Also quantitatively the energies are close to the values that have been computed in [38] with a different method restricted to axisymmetric shapes. Some final shapes including cuts through symmetry planes are displayed in Fig. 1.

4.3. Convergence experiment

The goal is now to numerically investigate our method with respect to convergence as the mesh is refined and as $\varepsilon \to 0$. We chose a rotationally symmetric configuration and relaxed a cigar of length 4 and diameter 1 with spherical caps and with symmetry axis $\{\boldsymbol{x} = (x_1,x_2,x_3)^T \in \mathbb{R}^3 | x_2 = x_3 = 0.5\}$. Area and enclosed volume are given by $A_1 + A_2 = 12.566356$ and $V = 2.879785$, respectively. We set $\alpha = 0$ and $\omega = 0.1$. The initial data for the order parameter were set to

$$c^0(\boldsymbol{x}) = \begin{cases} 1 & \text{if } 2.25 \leqslant x_1, \\ x_1 - 1.25 & \text{if } 0.25 \leqslant x_1 \leqslant 2.25, \\ -1 & \text{if } x_1 \geqslant 0.25, \end{cases} \quad \text{where } \boldsymbol{x} = (x_1,x_2,x_3)^T \in \mathbb{R}^3$$

and the area difference is given by $A_1 - A_2 = 4.71$. The initial configuration is displayed in Fig. 2 on the left. Simulations were performed on grids with between 2306 and 36,866 nodes. The initial grids were obtained by glueing together four coarsely triangulated surfaces of unit cubes, refining globally by bisection and projecting onto the surface. The following table lists the maximal and minimal initial edge lengths h^0_{max} and h^0_{min} as well as the (constant) time step $\tau = \tau^m$ for all m:

N_h	02306	04610	09218	18434	36866
h^0_{max}	0.143635	0.092185	0.076591	0.047842	0.039576
h^0_{min}	0.046909	0.036232	0.023239	0.018107	0.011182
$\tau/10^{-5}$	10.0	5.0	2.5	1.25	0.625

Since close to equilibrium the relaxation is rather slow an adaptive time stepping procedure is desirable but the method used in Section 4.2 on the pure Helfrich flow is not appropriate because of the contributions to the force coming from the line energy and because of the equation for the order parameter. This issue is left for future research but we remark that we performed simulations for various (constant) time steps indicating that the error from the time discretization is negligible compared to the spatial discretization error.

Fig. 3 shows typical evolutions of the velocity and the Lagrange multipliers. Initially, the evolution is rather fast. Later on, the quantities do not change any more in time, whence the system can be considered as relaxed. In Table 2 we present the

Table 1
Helfrich flow, results for several initial shapes where the parameters with the ellipsoids are the radii and with the cigars the diameter and the length. The cigars have been gently deformed towards prolates to initially comply with the constraints on area and volume. Energies have been normalized by dividing by $8\pi k_H$. From the phase diagram in [38, Fig. 8], values have been extracted for comparison. For the prolate/dumbbell branch with $\overline{V} = 0.7920$ as in the last row we performed another simulation on a finer grid resulting in a normalized energy of 1.4045.

Initial shape	N_h	$\overline{V}$	Final shape	$\mathcal{F}_h/(8\pi)$	[38]
Ellipsoid (0.85,0.85,0.23)	1538	0.6211	Discocyte	1.9010	1.9
Ellipsoid (0.7,0.7,0.2855)	1538	0.7921	Discocyte	1.4717	1.5
Cigar (0.7,3.5)	2818	0.6211	Dumbbell	1.9553	1.95
Cigar (0.7,2.1)	1794	0.7920	Dumbbell	1.4046	1.4

Please cite this article in press as: C.M. Elliott, B. Stinner, Modeling and computation of two phase geometric biomembranes using surface finite elements, J. Comput. Phys. (2010), doi:10.1016/j.jcp.2010.05.014

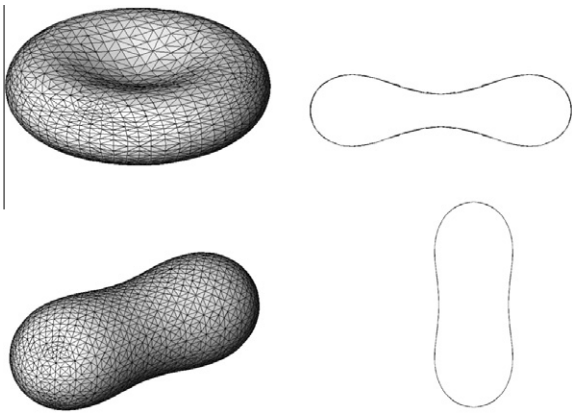

Fig. 1. Final shapes for the ellipsoid/discocyte branch with $\overline{V} \approx 0.62$ in the upper row and the prolate/dumbbell branch with $\overline{V} \approx 0.79$ in the lower row. In addition to the meshes, cuts through symmetry planes are displayed allowing for a qualitative comparison with shapes in [38, Fig. 9].

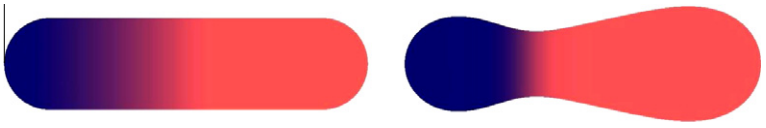

Fig. 2. Initial (left) and relaxed phase field surface (right, at time $t = 0.3$) for the convergences tests, here for $\varepsilon = 0.3$ and $N_h = 4610$ nodes. The color/grey-scale indicates the order parameter ranging from $c = 1$ (light red/grey), to $c = -1$ (dark blue/grey). (For interpretation of the references to colour in this figure legend, the reader is referred to the web version of this article.)

values for energy, the mass and the volume Lagrange multiplier, the velocity and the grid quality for $\varepsilon = 0.3$ measured at time $t = 0.3$. As has been mentioned, the influence of the time step is small compared to the influence of the number of nodes N_h. The values reveal convergence of $\mathcal{F}_h$, $\lambda_{c,h}$, $\lambda_{V,h}$, and $\|\boldsymbol{v}_h\|_{L^2} \to 0$ as $N_h \to \infty$.

Of further interest is the convergence as $\varepsilon \to 0$. We kept the ratio $\varepsilon/\sqrt{N_h}$ constant where the meshes are fine enough in the sense that a further refinement has negligible influence on the values compared to the influence of ε, i.e., the discretization error is smaller than the modeling error. The values are shown in Table 3. Fig. 4 displays the evolution of the membrane energy and (parts of the) shape profiles around the necks obtained by intersecting the plane $\{x_2 = 0.5\}$ with the surface. As $\varepsilon \to 0$ not only the energies converge but also the distance from one profile curve to the next one becomes smaller indicating that the surface shapes converge. We observed this not only in the displayed region but everywhere. The reason for zooming into this specific region is that the transition points marking the zero level sets of c_h are displayed, too, and apparently converge. This means that also the approximations to the interface locations converge as $\varepsilon \to 0$.

4.4. Test of the adaptive local grid refinement

By our choice of the double-well potential W the profile of the order parameter across an interfacial layer is close to $\tanh(d(\boldsymbol{x},t)/\varepsilon)$ where $d(\boldsymbol{x},t)$ is the geodesic distance of $\boldsymbol{x}$ to the level set $\{c(\boldsymbol{x},t) = 0\}$. If we define the interfacial layer to consist of the points $\{|c(\boldsymbol{x})| \leqslant 0.97\}$ then the thickness of the layer is close to 4ε. In our tests with the data of the previous section a value of $N_{in} = 1.6$ resulted in meshes with resolutions of the interfaces comparable with the fully refined meshes yielding the values in Table 3. With respect to the bulk a value of $N_H = 0.5$ resulted in a resolution of the phases comparable to the fully refined mesh with $N_h = 4610$ nodes close to the spherical tips and somewhat coarser in the cone-shaped part of the red phase. In Fig. 5 we compare the fully refined grid with the adaptively refined grid at time $t = 0.3$ for $\varepsilon = 0.3/\sqrt{2}$. In Table 4 the energies and the node numbers of the relaxed shapes for several values of ε are shown. The time step has been related to the element diameters in the interfacial regions and, hence, is the same for a given ε. Similarly as before our simulation results generally suggest that the discretization error is smaller than the modeling error (influence of ε).

4.5. Consistency with the phase diagram

We aimed for a quantitative comparison with the results in [32] for axisymmetric vesicles without area-difference term ($\alpha = 0$) but with a lateral phase separation. As initial data we chose prolate-like ellipsoids centered in the origin, symmetric with respect to the axis $\{\boldsymbol{x} = (x_1, x_2, x_3) \in \mathbb{R}^3 | x_1 = x_2 = 0\}$, with pronounced tips in x_3-direction and with appropriate radii to

Please cite this article in press as: C.M. Elliott, B. Stinner, Modeling and computation of two phase geometric biomembranes using surface finite elements, J. Comput. Phys. (2010), doi:10.1016/j.jcp.2010.05.014

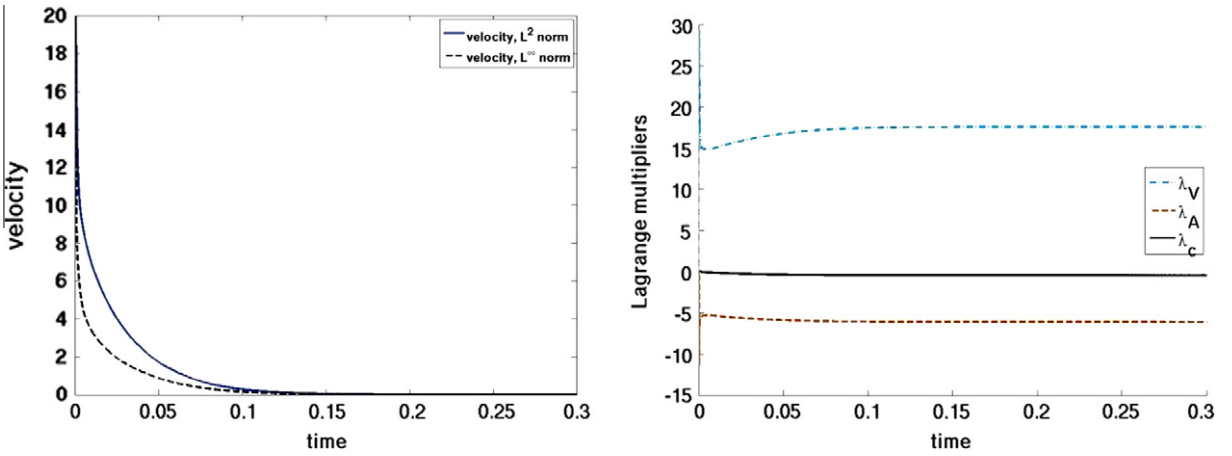

Fig. 3. Relaxation of cigars with two phases. For $\varepsilon = 0.3$ on the mesh with $N_h = 4610$ nodes we display the evolution of $\|\boldsymbol{\nu}_h\|_{L^2(\Gamma_h)}$ and $\|\boldsymbol{\nu}_h\|_{L^\infty(\Gamma_h)}$ on the left and the evolution of the Lagrange multipliers on the right.

Table 2
Convergence tests with cigars relaxing to non-symmetric dumbbells as in Fig. 2, values at time $t = 0.3$ for $\varepsilon = 0.3$.

N_h	$\mathcal{F}_h$	$\lambda_{c,h}$	$\lambda_{V,h}$	$\|\boldsymbol{\nu}_h\|_{L^2(\Gamma_h)}$	q
02306	49.898116	−0.440981	17.568521	0.01961168	0.435407
04610	49.893313	−0.439833	17.572988	0.00844491	0.430948
09218	49.892998	−0.439936	17.572570	0.00556093	0.426217
18434	49.892651	−0.439907	17.572540	0.00165041	0.424645

Table 3
Convergence tests with cigars relaxing to non-symmetric dumbbells as in Fig. 2, values at time $t = 0.3$ and experimental errors of convergence computed according to (4.2).

ε	N_h	$\mathcal{F}_h$	*eoc*	$\lambda_{c,h}$	*eoc*	$\lambda_{V,h}$	*eoc*
0.3	04610	49.8933	–	−0.4399	–	17.5725	–
$0.3/\sqrt{2}$	09218	49.8104	1.2511	−0.4598	1.5139	17.5797	1.1018
0.15	18434	49.7567	1.6448	−0.4716	1.7940	17.5845	2.3746
$0.15/\sqrt{2}$	36866	49.7262	–	−0.4779	–	17.5867	–

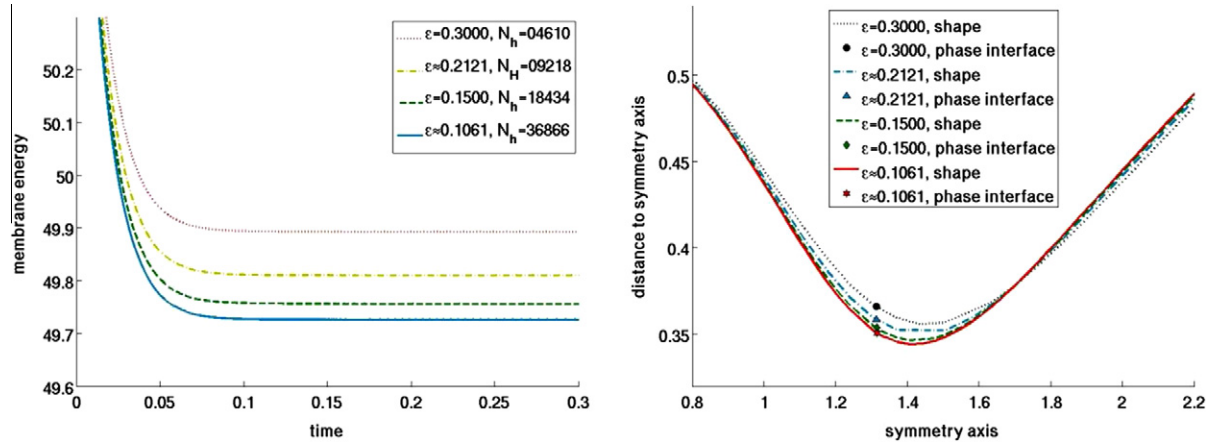

Fig. 4. Relaxation of cigars with two phases. On the left: evolution of the membrane energy $\mathcal{F}_h$ for different values of ε. On the right: shape profiles as in Fig. 2 (right) around the necks with the phase transition region for several values of ε; we display the distance in the x_3-direction of the surface to the symmetry axis $\{x_2 = x_3 = 0.5\}$ and the position of the phase interface characterized by $c_h = 0$; we remark that the axes scale differently.

Please cite this article in press as: C.M. Elliott, B. Stinner, Modeling and computation of two phase geometric biomembranes using surface finite elements, J. Comput. Phys. (2010), doi:10.1016/j.jcp.2010.05.014

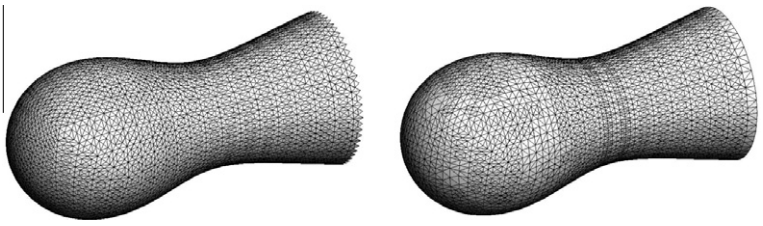

Fig. 5. Parts of the meshes of relaxed shapes for the test data in Section 4.3 with $\varepsilon = 0.3/\sqrt{2}$, fully refined mesh with $N_h = 9218$ nodes (left) in comparison with the adaptively refined mesh with $N_h = 6114$ nodes (right).

fulfill the constraint on the given reduced volume $\overline{V}$ (recall Section 4.2 for its definition; the characteristic length scales $\overline{R}$ were about 1.9). The initial values for the order parameter where of the form

$$c^0(\boldsymbol{x}) = \begin{cases} 1 & \text{if } p + 0.25 \leqslant x_3, \\ 4(x_3 - p) & \text{if } p - 0.25 \leqslant x_3 \leqslant p + 0.25, \\ -1 & \text{if } x_3 \leqslant p - 0.25, \end{cases}$$

where $\boldsymbol{x} = (x_1, x_2, x_3)^T \in \mathbb{R}^3$ with an appropriate value p for the height of the interface such that the first phase occupies a tenth of the total domain, $A_1/(A_1 + A_2) = 0.1$. Further, we set $\omega = 0.1$. The computations have been carried out with adaptive mesh refinement and the results are displayed in Table 5 revealing a good agreement with the values in [32].

4.6. Effects from the non-local bending energy

We now present a computational example that demonstrates the effectivity of our method for non-axisymmetric shapes. The initial shape shown in Fig. 6 on the left has a minimal edge length of $h^0_{min} \approx 0.055$ and the all simulations have been carried out with a fixed time step of $\tau = 4.0 \times 10^{-5}$.

Neglecting any phase separation phenomena we first relaxed the initial shape under the Helfrich flow with area-difference term ($\alpha = 100$). The resulting shape is non-axisymmetric and shown in Fig. 6 on the right which qualitatively is in agreement with the results in [41].

In turn, when relaxing the same shape without the area-difference term ($\alpha = 0$) then the resulting shape is axisymmetric again but involves an unphysical self-intersection. In Fig. 7 we display some shapes during the relaxation.

Finally we took a phase separation with an initial field c^0 into account that involved a red phase at one of the tips and blue phases elsewhere, see Fig. 8 on the left for the initial shape with order parameter and on the right for the relaxed shape. Apart from additional parameters for the phase separation the simulation parameters were the same as before in Fig. 6. As expected, the energy associated with the phase interface leads to a more pronounced neck between the tip with the red phase and the remainder of the vesicle in the blue phase.

4.7. Two-phase discocytes

We investigate the effect of a phase separation on a discocyte shape as in Fig. 1 (top). The initial configuration is displayed in Fig. 9 on the top which is a discocyte centered at the origin and with symmetry axis $\{(0, 0, z) \in \mathbb{R}^3 | z \in \mathbb{R}\}$. The initial values for the order parameter were of the form

$$c^0(\boldsymbol{x}) = \begin{cases} 1 & \text{if } 0.4 \leqslant x_3, \\ 5x_0 - 1 & \text{if } 0.0 \leqslant x_3 \leqslant 0.4, \\ -1 & \text{if } x_3 \leqslant 0.0, \end{cases} \qquad \text{where } \boldsymbol{x} = (x_1, x_2, x_3)^T \in \mathbb{R}^3.$$

The simulation data is shown in the caption to Fig. 9. In particular, the reduced volume is $\overline{V} \approx 0.6297$.

Table 4
Comparison of numbers of nodes, energy, and Lagrange multipliers for the volume constraint in dependence of ε for the fully and adaptively refined meshes (with strategy $(N_{in}, N_{off}, N_H) = (1.6, 0.1, 0.5)$), test problem as described in Section 4.3, values measured at time at time $t = 0.3$.

ε	Fully refined mesh			Adaptively refined mesh		
	N_h	$\mathcal{F}_h$	$\lambda_{V,h}$	N_h	$\mathcal{F}_h$	$\lambda_{V,h}$
0.3	04610	49.893313	17.572988	03698	49.893365	17.573109
$0.3/\sqrt{2}$	09218	49.810412	17.579676	06114	49.809644	17.580724
0.15	18434	49.756678	17.584547	06786	49.756712	17.584635
$0.15/\sqrt{2}$	36866	49.726291	17.586686	09850	49.725234	17.586805
0.075	–	–	–	09914	49.708009	17.585037

Please cite this article in press as: C.M. Elliott, B. Stinner, Modeling and computation of two phase geometric biomembranes using surface finite elements, J. Comput. Phys. (2010), doi:10.1016/j.jcp.2010.05.014

Table 5
Quantitative comparison between the energies extracted from the phase diagram in Section II.B.2 on p. 2676 in [32] and the energies measured with our method. In the last row the result for a larger ε than in the third row but the same parameters otherwise reveals a bigger energy. In the test example in Section 4.3 we had already observed that decreasing ε leads to decay of the energy, cf. Table 3.

red. vol.	Extracted	$\mathcal{F}_h/(8\pi)$	ε
0.95	2.22	2.222	0.1
0.91	2.175	2.177	0.1
0.90	2.155	2.157	0.1
0.89	2.11	2.124	0.1
0.90	2.155	2.1614	0.15

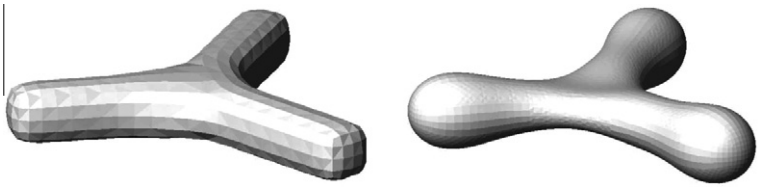

Fig. 6. Initial (left) and relaxed (right) shape for the Helfrich flow with weak area-difference constraint ($\alpha = 100$, $c \equiv 1$). Simulation parameters are $V = 8.513298, A_1 + A_2 = 33.931229, A_1 - A_2 = -23.6, M_0 = m_0\overline{R} = 69.0$, and we set $k_H = 1.0$. The length scale is $\overline{R} \approx 1.643$ and the reduced volume $\overline{V} \approx 0.458$. At the end time $t = 2.0$ we had $N_h = 4170$ grid points and a total energy of $\mathcal{F}_h \approx 81.752518$ with a main contribution of $\mathcal{F}_W^h \approx 81.749575$ from the bending energy and a small contribution of $\mathcal{F}_M^h \approx 0.002943$ from the area-difference term.

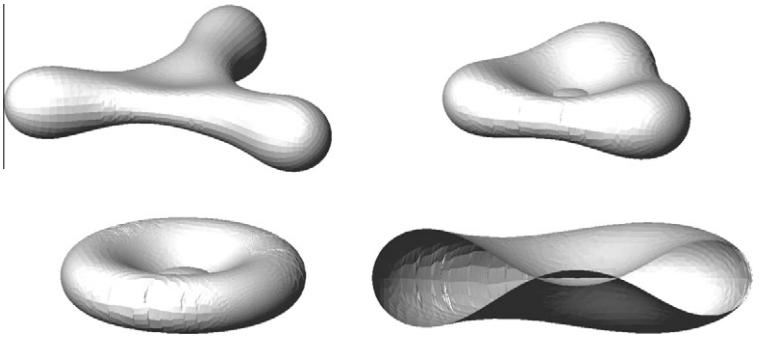

Fig. 7. Relaxation of the initial shape in Fig. 6 (left) subject to Helfrich flow ($\alpha = 0$, $c \equiv 1$). The shapes are displayed at times $t = 0.2$ (upper left, very similar to the relaxed shape with $\alpha = 100$, see Fig. 6 on the right), $t = 0.4$ (upper right, revealing already a self-intersection), and $t = 1.0$ (lower left, axisymmetric relaxed shape), and on the lower right we show a cut through the middle of the shape at time $t = 0.5$ more clearly revealing a self-intersection. Simulation parameters are $V = 8.513298$, $A_1 + A_2 = 33.931229$, and we set $k_H = 1.0$. The length scale is $\overline{R} \approx 1.643$ and the reduced volume $\overline{V} \approx 0.458$.

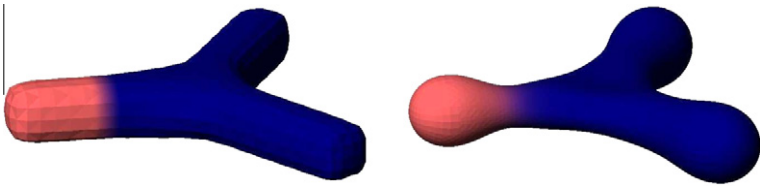

Fig. 8. Initial (left) and relaxed (right) shape for membrane energy with phase separation and area-difference constraint ($\alpha = 100$). Simulation parameters are $V = 8.513298, A_1 + A_2 = 33.931229, A_1 - A_2 = -23.6, M_0 = m_0\overline{R} = 69.0$, and we set $\sigma = 2$, $k_H = 1$, $\omega = 0.02$, $\varepsilon = 0.4$. The length scale is $\overline{R} \approx 1.643$ and the reduced volume $\overline{V} \approx 0.458$. At the end time $t = 2.0$ we had $N_h = 4746$ grid points, and energy contributions of $\mathcal{F}_W^h \approx 83.171314, \mathcal{F}_{GL}^h \approx 6.373348$, and $\mathcal{F}_M^h \approx 0.001882$. The color/grey-scale indicates the order parameter ranging from $c = 1$ (light red/grey) to $c = -1$ (dark blue/grey). (For interpretation of the references to colour in this figure legend, the reader is referred to the web version of this article.)

As σ is increased from zero the equilibrium discocyte is deformed maintaining some non-convex portions. For instance, the relaxed shape for $\sigma = 3$ in Fig. 9 in the middle still reveals dents. However if σ is increased to $\sigma = 3.45$ then the dents

Please cite this article in press as: C.M. Elliott, B. Stinner, Modeling and computation of two phase geometric biomembranes using surface finite elements, J. Comput. Phys. (2010), doi:10.1016/j.jcp.2010.05.014

vanish and the final shape is an axisymmetric dumbbell shape but with a different symmetry axis to that of the initial discocyte, namely $\{(x,0,0) \in \mathbb{R}^3 | x \in \mathbb{R}\}$, see Fig. 9 on the bottom.

For comparison we also performed simulations with cigar-like initial shapes and the same simulation parameters. In this range (recall that $\overline{V} \approx 0.6297$) we know from Section 4.2 that shapes belonging to the oblate/discocyte branch energetically are favorable, hence we expect this to hold for small σ. In Fig. 10 we show plots of the energies of the relaxed shapes over σ where we obtain the dashed curve when relaxing an initial cigar shape and the continuous curve when relaxing the discocyte. The latter one indeed reveals less energy for σ up to about 0.8. After that, the shapes belonging to the prolate/dumbbell branch have less energy, and for $\sigma \geqslant 3.45$ the discocytes also relax to shapes of this branch. That we obtain two-phase discocytes as in the middle of Fig. 9 for σ between 0.8 and 3.45 indicates that these shapes are local minimizers of the membrane energy since the relaxation method ensures that the energy decays.

4.8. Topological changes of the phase separation

In the previous example it was mainly the initial membrane shape which lead to different relaxed shapes for the same parameters. We now consider an example where such an effect is due to the initial location of the interphase boundary.

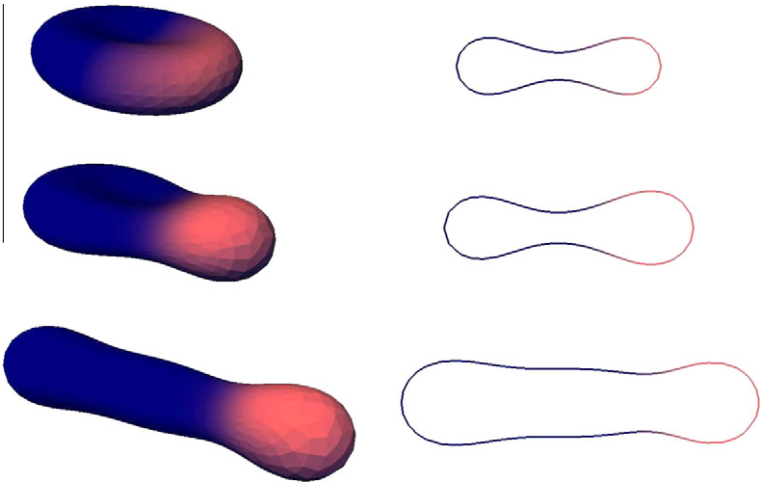

Fig. 9. Relaxation of a discocyte with phase separation. From top to bottom: initial shape and final shapes for $\sigma = 3, 4$ a time $t = 0.03$ on the left, on the right the corresponding cross-sections through the plane $\{\boldsymbol{x} \in \mathbb{R}^3 | x_1 = 0\}$. Further simulation parameters are $V = 0.179394$, $A_1 + A_2 = 2.093816$, $A_1 - A_2 = -0.917461$, $\alpha = 0, k_H = 1$, $\omega = 0.02, \varepsilon = 0.1$. The length scale is $\overline{R} \approx 0.408$ and the reduced volume $\overline{V} \approx 0.6297$. The color/grey-scale indicates the order parameter ranging from $c = 1$ (light red/grey) to $c = -1$ (dark blue/grey). (For interpretation of the references to colour in this figure legend, the reader is referred to the web version of this article.)

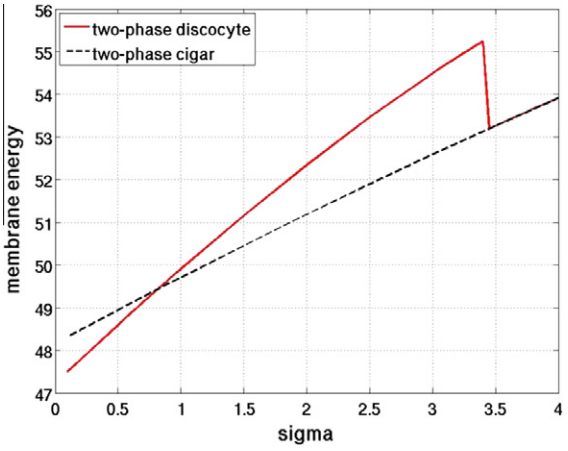

Fig. 10. Energies of relaxed two-phase membranes from the oblate/discocyte branch (cf. Fig. 9) versus the prolate/dumbbell branch (cf. Fig. 2) plotted over σ. Parameters are $V = 0.179394$, $A_1 + A_2 = 2.093816$, $A_1 - A_2 = -0.917461$, $\alpha = 0, k_H = 1$, $\varepsilon = 0.1$. The length scale is $\overline{R} \approx 0.408$ and the reduced volume $\overline{V} \approx 0.6297$.

Please cite this article in press as: C.M. Elliott, B. Stinner, Modeling and computation of two phase geometric biomembranes using surface finite elements, J. Comput. Phys. (2010), doi:10.1016/j.jcp.2010.05.014

We consider cigar-like shapes. The domain of one phase is an annular region around its cylindrical portion but the heights are different, see Figs. 11 and 12 on the left. The simulation parameters are given in the captions of these Figures and are identical for the two simulations.

For the higher positioned phase interfaces of Fig. 11 we observe that the dark blue/grey phase detects the tip and moves there resulting in two connected inter-membrane phases and a total energy of $\mathcal{F}_h \approx 52.1334$. In turn, the two light red/grey domains remain separated by the annular dark blue/grey domain of the other phase when the phase interfaces initially are positioned further away from the upper tip, see Fig. 12. The final energy in the latter case is $\mathcal{F}_h \approx 55.145$ and bigger than in

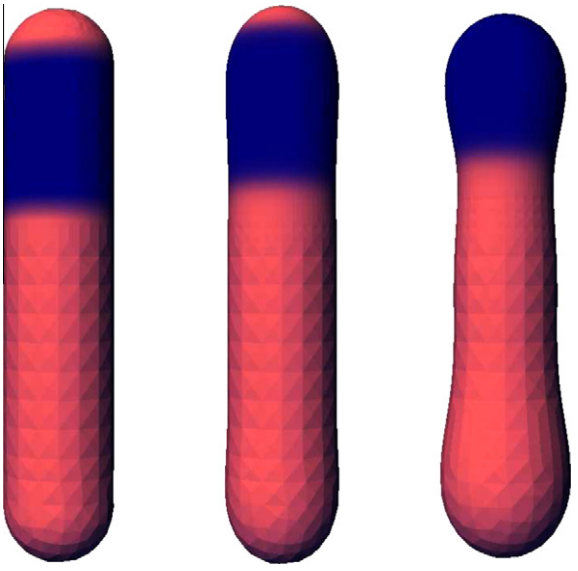

Fig. 11. Relaxation of a cigar-like initial shape with two circular phase interfaces, on the left at time $t = 0.0$, in the middle at time $t = 0.000075$ and on the right the relaxed shape a time $t = 0.005$. Further simulation parameters are $V = 0.307931$, $A_1 + A_2 = 3.013179$, $A_1 - A_2 = 1.36198$, $\alpha = 0$, $k_H = 1$, $\sigma = 2$,$\omega = 0.001$, $\varepsilon = 0.05$. The length scale is $\overline{R} \approx 0.4897$ and the reduced volume $\overline{V} \approx 0.6261$. The color/grey-scale indicates the order parameter ranging from $c = 1$ (light red/grey) to $c = -1$ (dark blue/grey). (For interpretation of the references to colour in this figure legend, the reader is referred to the web version of this article.)

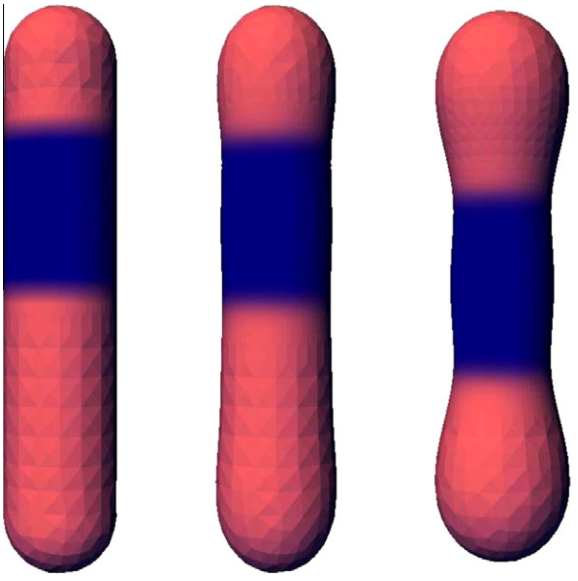

Fig. 12. Relaxation of a cigar-like initial shape with two circular phase interfaces, on the left at time $t = 0.0$, in the middle at time $t = 0.00025$ and on the right the relaxed shape a time $t = 0.005$. Further simulation parameters are $V = 0.307931$, $A_1 + A_2 = 3.013179$, $A_1 - A_2 = 1.36198$, $\alpha = 0$, $k_H = 1$, $\sigma = 2$, $\omega = 0.001$, $\varepsilon = 0.05$. The length scale is $\overline{R} \approx 0.4897$ and the reduced volume $\overline{V} \approx 0.6261$. The color/grey-scale indicates the order parameter ranging from $c = 1$ (light red/grey) to $c = -1$ (dark blue/grey). (For interpretation of the references to colour in this figure legend, the reader is referred to the web version of this article.)

Please cite this article in press as: C.M. Elliott, B. Stinner, Modeling and computation of two phase geometric biomembranes using surface finite elements, J. Comput. Phys. (2010), doi:10.1016/j.jcp.2010.05.014

the previous case because the phase interface has approximately twice the length. In fact, the line energy of the relaxed shape in Fig. 12 on the right is $\mathcal{F}^h_{GL} \approx 6.4135$ whilst the shape in Fig. 11 on the right involves a line energy of $\mathcal{F}^h_{GL} \approx 3.3271$.

Acknowledgments

The second author thanks the German Research Foundation (DFG) for financial support with Grant STI 579/1-1,2. Also this research has been supported by the UK Engineering and Physical Sciences Research Council (EPSRC), Grant EP/G010404.

Appendix A. Notation and concepts

A.1. Calculus on evolving surfaces

To represent membranes we consider smooth oriented two-dimensional hypersurfaces $\Gamma \subset \mathbb{R}^3$ which have non-empty smooth boundaries $\partial\Gamma$ and which can be parameterized by maps $\boldsymbol{y} : \mathcal{M} \to \Gamma$ over two-dimensional reference manifolds $\mathcal{M}$. To fix the orientation let $\boldsymbol{\nu}$ denote a unit normal field on Γ. Later on we will consider surfaces that are the boundary of a domain $\Omega \subset \mathbb{R}^3$ and then $\boldsymbol{\nu}$ will be the external unit normal. Here, we just pick any orientation. Further, let $\boldsymbol{\mu}$ denote the outer co-normal of Γ on $\partial\Gamma$.

To discuss the surface gradient we may consider a fixed surface Γ. For any function η defined on a neighborhood of $\mathcal{N} \subset \mathbb{R}^3$ of Γ we define its tangential gradient on Γ by

$$\nabla_\Gamma \eta := \nabla \eta - \nabla \eta \cdot \boldsymbol{\nu}\boldsymbol{\nu}$$

where $\cdot$ denotes the standard scalar product and $\nabla\eta$ denotes the usual gradient on $\mathbb{R}^3$. The tangential gradient $\nabla_\Gamma\eta$ only depends on the values of η restricted to Γ, and $\nabla_\Gamma\eta \cdot \boldsymbol{\nu} = 0$. The components of the tangential gradient will be denoted by $\nabla_\Gamma \eta = (\underline{D}_i \eta)_{i=1}^3$. If $\boldsymbol{w} : \Gamma \to \mathbb{R}^3$ is a smooth vector field then $\nabla_\Gamma \boldsymbol{w}$ is the matrix with components $(\nabla_\Gamma \boldsymbol{w})_{ij} = \underline{D}_j \boldsymbol{w}_i$, and we write $(\nabla_\Gamma \boldsymbol{w})^T = (\underline{D}_i \boldsymbol{w}_j)_{i,j}$ for its transpose and use the scalar product $\nabla_\Gamma \boldsymbol{w} : \nabla_\Gamma \boldsymbol{z} = \sum_{i,j} \underline{D}_j \boldsymbol{w}_i \underline{D}_j \boldsymbol{z}_i$. We will furthermore use the notation $\boldsymbol{w} \otimes \boldsymbol{z}$ for the matrix with entries $w_i z_j$. The surface divergence is defined by $\nabla_\Gamma \cdot \boldsymbol{w} = \mathrm{tr}(\nabla_\Gamma \boldsymbol{w})$. The Laplace–Beltrami operator on $\Gamma(t)$ is defined as the tangential divergence of the tangential gradient, $\Delta_\Gamma \eta = \nabla_\Gamma \cdot \nabla_\Gamma \eta$.

At a point $\boldsymbol{x} \in \Gamma$ we define the matrix $\boldsymbol{P}(\boldsymbol{x}) := \boldsymbol{I} - \boldsymbol{\nu}(\boldsymbol{x}) \otimes \boldsymbol{\nu}(\boldsymbol{x}) \in \mathbb{R}^{3\times 3}$ where $\boldsymbol{I}$ is the identity matrix. Any vector $\boldsymbol{y} \in \mathbb{R}^3$ is projected by $\boldsymbol{P}$ to the tangent space $T_{\boldsymbol{x}}\Gamma$. With the help of $\boldsymbol{P}$ we can write

$$\nabla_\Gamma \eta = \boldsymbol{P}\nabla\eta, \quad \nabla_\Gamma \boldsymbol{w} = \nabla \boldsymbol{w}\boldsymbol{P}, \quad \nabla_\Gamma \cdot \boldsymbol{w} = \boldsymbol{P} : \nabla_\Gamma \boldsymbol{w}. \tag{A.1}$$

Let $\mathcal{I}_\Gamma : \Gamma \to \Gamma, \mathcal{I}_\Gamma(\boldsymbol{x}) = \boldsymbol{x}$ for all $\boldsymbol{x} \in \Gamma$, denote the identity map on surface Γ. Throughout this paper we will usually simply write $\boldsymbol{x}$ for the identity map on (the actual surface) Γ. After extending $\mathcal{I}_\Gamma$ to $\mathcal{N}$, the identities $\nabla \mathcal{I}_\Gamma = \nabla \boldsymbol{x} = \boldsymbol{I}$ and (A.1) yield that $\nabla_\Gamma \boldsymbol{x} = \nabla \boldsymbol{x}\boldsymbol{P} = \boldsymbol{P} = \boldsymbol{I} - \boldsymbol{\nu} \otimes \boldsymbol{\nu}$.

The mean curvature of Γ with respect to $\boldsymbol{\nu}$ is defined by

$$H = \nabla_\Gamma \cdot \boldsymbol{\nu}. \tag{A.2}$$

Observe that the orientation is such that if Γ is the boundary of a ball of radius R and $\boldsymbol{\nu}$ its external unit normal then its mean curvature is $H = \frac{2}{R}$. Note that H is the sum of the principle curvatures rather than the arithmetic mean and hence differs from the common definition by a factor 2. We remark that the mean curvature vector $\boldsymbol{H} = H\boldsymbol{\nu}$ is invariant with respect to the orientation of $\boldsymbol{\nu}$, and the identity (1.8) follows from

$$\Delta_\Gamma \boldsymbol{x} = \nabla_\Gamma \cdot \nabla_\Gamma \boldsymbol{x} = \nabla_\Gamma \cdot \boldsymbol{P} = -\nabla_\Gamma \cdot \boldsymbol{\nu}\boldsymbol{\nu} = -H\boldsymbol{\nu}.$$

As observed by Dziuk [17,18], the following variational identity is useful in defining numerical schemes and in the variational calculus:

Definition A. 1 (*Variational curvature equation*). For a smooth closed surface Γ with mean curvature H the following weak equation holds for the identity map

$$\int_\Gamma \boldsymbol{H} \cdot \boldsymbol{z} - \nabla_\Gamma \boldsymbol{x} : \nabla_\Gamma \boldsymbol{z} = 0 \tag{A.3}$$

for each test vector field $\boldsymbol{z} : \Gamma \to \mathbb{R}^3$.

For each surface $\Gamma(\cdot)$, the symmetric matrix $\nabla_\Gamma \boldsymbol{\nu}$ of the tangential derivatives of the normal field is known as the Weingarten map or shape operator. It satisfies $|\nabla_\Gamma \boldsymbol{\nu}|^2 = H_1^2 + H_2^2 = H^2 - 2K$ where H_i are the principle curvatures, $H = H_1 + H_2$ and $K = H_1 H_2$ is the Gaussian curvature.

There is a formula for partial integration:

$$\int_\Gamma \nabla_\Gamma \eta = \int_\Gamma \eta H \boldsymbol{\nu} + \int_{\partial\Gamma} \eta \boldsymbol{\mu}. \tag{A.4}$$

Please cite this article in press as: C.M. Elliott, B. Stinner, Modeling and computation of two phase geometric biomembranes using surface finite elements, J. Comput. Phys. (2010), doi:10.1016/j.jcp.2010.05.014

Let us write γ for a smooth curve on Γ or the boundary of Γ and let $\boldsymbol{\tau}_\gamma$ denote the unit tangential field along γ such that $(\boldsymbol{\tau}_\gamma, \boldsymbol{\mu}, \boldsymbol{\nu})$ constitutes a positively oriented orthonormal basis in every point on γ. The notation $\nabla_\gamma f$ stands for the derivative of a field $f : \gamma \to \mathbb{R}$ along γ: Using a parameterization $\boldsymbol{r}(s)$ for curve γ we have that

$$\nabla_\gamma f = \frac{1}{|\partial_s \boldsymbol{r}(s)|} \partial_s (f \circ \boldsymbol{r})(s) \boldsymbol{\tau}_\gamma.$$

The curvature vector of γ is denoted by $\boldsymbol{h}$ and fulfills

$$\boldsymbol{h} = \frac{1}{|\partial_s \boldsymbol{r}(s)|} \partial_s \left(\frac{\partial_s \boldsymbol{r}(s)}{|\partial_s \boldsymbol{r}(s)|} \right). \tag{A.5}$$

It is normal to the curve whence we may write

$$\boldsymbol{h} = h_g \boldsymbol{\mu} + h_\nu \boldsymbol{\nu}.$$

The quantity $h_g = \boldsymbol{h} \cdot \boldsymbol{\mu}$ is the *geodesic curvature* of γ and $h_\nu = \boldsymbol{h} \cdot \boldsymbol{\nu}$ is usually called *normal curvature* (with respect to Γ).

A.2. The material derivative and transport formulae

Relaxing an initial surface by deforming it leads to the notion of an evolving surface $\{\Gamma(t)\}_t$ depending smoothly on the time $t \in I := [0, \infty)$, i.e., the parameterizations $\boldsymbol{y}(\cdot, t) : \mathcal{M} \to \Gamma(t)$ depend smoothly on t. We define the velocity of $\Gamma(t)$ in a point $\boldsymbol{y}(p,t)$ with $p \in \mathcal{M}$ by

$$\boldsymbol{v}(\cdot, t) : \Gamma(t) \to \mathbb{R}^3, \quad \boldsymbol{v}(\boldsymbol{y}(p,t), t) := \frac{d}{dt} \boldsymbol{y}(p,t).$$

Interpreting $\boldsymbol{y}(p,t)$ as a mass point the velocity vector field may be understood as the material velocity. In general, one can decompose the velocity into the form $\boldsymbol{v} = v_\nu \boldsymbol{\nu} + \boldsymbol{v}_\tau$ with a scalar normal component $v_\nu := \boldsymbol{v} \cdot \boldsymbol{\nu}$ and a tangential vector field $\boldsymbol{v}_\tau := \boldsymbol{v} - v_\nu \boldsymbol{\nu}$.

We will usually omit the dependence of fields and surfaces on t since it is clear from the context whether we deal with the evolving surface or a surface at a specific time. In particular, we just write ∇_Γ for $\nabla_{\Gamma(t)}$ whence this operator contains only spatial derivatives but no time derivatives.

By $\partial_t^\bullet$ we denote the *material derivative* of a scalar function $\eta = \eta(\boldsymbol{x}, t)$ defined on an open set around the moving surface, $\partial_t^\bullet \eta = \frac{\partial \eta}{\partial t} + \boldsymbol{v} \cdot \nabla \eta$. Recalling the parameterizations $\boldsymbol{y}(t)$ we note that

$$\partial_t^\bullet \eta(\boldsymbol{y}(t), t) = \frac{d}{dt} \eta(\boldsymbol{y}(\cdot), \cdot)|_t = \partial_t \eta(\boldsymbol{y}(t), t) + \boldsymbol{v}(\boldsymbol{y}(t), t) \cdot \nabla \eta(\boldsymbol{y}(t), t) \tag{A.6}$$

from which we see that the material derivative depends only on the values of η on the surface $\Gamma(t)$. Occasionally we will also use the *normal time derivative* where only the normal portion of the velocity is taken into account:

$$\partial_t^\circ \eta(\boldsymbol{y}(t), t) = \partial_t \eta(\boldsymbol{y}(t), t) + v_\nu(\boldsymbol{y}(t), t) \frac{\partial \eta}{\partial \boldsymbol{\nu}}(\boldsymbol{y}(t), t). \tag{A.7}$$

In the problem that we will consider later on the velocity field is purely normal, and in this case material derivative and normal time derivative coincide. In the general case, a consequence of the splitting of $\boldsymbol{v}$ into a normal and a tangential part is the relation $\partial_t^\bullet \eta = \partial_t^\circ \eta + \boldsymbol{v}_\tau \cdot \nabla_\Gamma \eta$. It is convenient to note that with (A.2) we obtain

$$\nabla_\Gamma \cdot \boldsymbol{v} = \nabla_\Gamma \cdot (v_\nu \boldsymbol{\nu}) + \nabla_\Gamma \cdot \boldsymbol{v}_\tau = v_\nu \nabla_\Gamma \cdot \boldsymbol{\nu} + \nabla_\Gamma \cdot \boldsymbol{v}_\tau = v_\nu H + \nabla_\Gamma \cdot \boldsymbol{v}_\tau. \tag{A.8}$$

The following formulae for the differentiation of a parameter dependent surface integral will play a decisive role.

Lemma A.2 (Transport formulae). *Let $\{\Gamma(t)\}_{t \in I}$ be an evolving surface and η, ψ be smooth scalar fields on Γ such that all the following integrals exist. Then*

$$\frac{d}{dt} \int_\Gamma \eta = \int_\Gamma (\partial_t^\bullet \eta + \eta \nabla_\Gamma \cdot \boldsymbol{v}). \tag{A.9}$$

Further, with the rate of deformation tensor $D(\boldsymbol{v})_{ij} = \frac{1}{2}(\underline{D}_i \boldsymbol{v}_j + \underline{D}_j \boldsymbol{v}_i)$ $(i,j = 1, \ldots, n)$,

$$\frac{d}{dt} \int_\Gamma \nabla_\Gamma \eta \cdot \nabla_\Gamma \psi = \int_\Gamma \nabla_\Gamma \psi \cdot \nabla_\Gamma \partial_t^\bullet \eta + \int_\Gamma \nabla_\Gamma \partial_t^\bullet \psi \cdot \nabla_\Gamma \eta + \int_\Gamma \nabla_\Gamma \eta \cdot (\nabla_\Gamma \cdot \boldsymbol{v} - 2D(\boldsymbol{v})) \nabla_\Gamma \psi. \tag{A.10}$$

A proof of this Lemma is given in [19].

Later on we will apply (A.10) with η and ψ replaced by the components of the vector field $\boldsymbol{x}$ and another vector field $\boldsymbol{z}$, respectively. Then we will also apply the following identity which is derived using (A.1) and that $\boldsymbol{P} = \nabla_\Gamma \boldsymbol{x}$ is symmetric (here, the summation convention is employed):

$$\begin{aligned} \nabla_\Gamma \boldsymbol{x}_i \cdot 2D(\boldsymbol{v}) \nabla_\Gamma \boldsymbol{z}_i &= \underline{D}_j \boldsymbol{x}_i \underline{D}_j \boldsymbol{v}_k \underline{D}_k \boldsymbol{z}_i + \underline{D}_j \boldsymbol{x}_i \underline{D}_k \boldsymbol{v}_j \underline{D}_k \boldsymbol{z}_i = \underline{D}_k \boldsymbol{z}_i \underline{D}_j \boldsymbol{v}_k \underline{D}_i \boldsymbol{x}_j + \underline{D}_i \boldsymbol{x}_j \underline{D}_k \boldsymbol{z}_i \underline{D}_k \boldsymbol{v}_j \\ &= ((\nabla_\Gamma \boldsymbol{z})^T)_{ki} (\nabla_\Gamma \boldsymbol{v} \nabla_\Gamma \boldsymbol{x})_{ki} + (\nabla_\Gamma \boldsymbol{x} \nabla_\Gamma \boldsymbol{z})_{jk} (\nabla_\Gamma \boldsymbol{v})_{jk} = (\nabla_\Gamma \boldsymbol{z})^T : \nabla_\Gamma \boldsymbol{v} + \boldsymbol{P} \nabla_\Gamma \boldsymbol{z} : \nabla_\Gamma \boldsymbol{v}. \end{aligned} \tag{A.11}$$

Please cite this article in press as: C.M. Elliott, B. Stinner, Modeling and computation of two phase geometric biomembranes using surface finite elements, J. Comput. Phys. (2010), doi:10.1016/j.jcp.2010.05.014

Further useful formulae for time derivatives of the unit normal are

$$\partial_t^\circ \boldsymbol{\nu} = -\nabla_\Gamma(\boldsymbol{v}\cdot\boldsymbol{\nu}) = -\nabla_\Gamma v_\nu, \quad \partial_t^\bullet \boldsymbol{\nu} = -(\nabla_\Gamma \boldsymbol{v})^T \boldsymbol{\nu}. \tag{A.12}$$

For the first identity we refer to [26]. The second one follows from the first one and the fact that $\nabla_\Gamma \boldsymbol{v}$ is tangential and symmetric:

$$\partial_t^\bullet \boldsymbol{\nu} = \partial_t^\circ \boldsymbol{\nu} + \nabla_\Gamma \boldsymbol{\nu}\boldsymbol{v}_\tau = -\nabla_\Gamma(\boldsymbol{v}\cdot\boldsymbol{\nu}) + \nabla_\Gamma \boldsymbol{\nu}\boldsymbol{v} = -(\nabla_\Gamma \boldsymbol{v})^T \boldsymbol{\nu} - (\nabla_\Gamma \boldsymbol{\nu})^T \boldsymbol{v} + (\nabla_\Gamma \boldsymbol{\nu})^T \boldsymbol{v}.$$

References

[1] D. Andelman, T. Kawakatsu, K. Kawasaki, Equilibrium shape of two-component unilamellar membranes and vesicles, Europhys. Lett. 19 (1992) 57–62.
[2] J.W. Barrett, H. Garcke, R. Nürnberg, Parametric approximation of Willmore flow and related geometric evolution equations, SIAM J. Sci. Comput. 31 (2008) 225–253.
[3] T. Baumgart, S. Hess, W. Webb, Imaging coexisting fluid domains in biomembrane models coupling curvature and line tension, Nature 425 (2003) 821–824.
[4] T. Baumgart, S.L. Das, W. Webb, J. Jenkin, Membrane elasticity in giant vesicles with fluid phase coexistence, Biophys. J. 89 (2005) 1067–1084.
[5] T. Biben, C. Misbah, Tumbling of vesicles under shear flow within an advected-field approach, Phys. Rev. E 67 (2003) 031908-1–031908-5.
[6] T. Biben, K. Kassner, C. Misbah, Phase-field approach to three-dimensional vesicle dynamics, Phys. Rev. E 72 (2005) 041921-1–041921-15.
[7] M. Bloor, M. Wilson, Method for efficient shape parametrization of fluid membranes and vesicles, Phys. Rev. E 61 (2000) 4218–4229.
[8] A. Bobenko, P. Schröder, Discrete Willmore flow, in: M. Desbrun, H. Pottmann (Eds.), Eurographics Symp. Geom. Processing, 2005.
[9] A. Bonito, R.H. Nochetto, M.S. Pauletti, Parametric FEM for geometric biomembranes, J. Comput. Phys. 229 (2010) 3171–3188.
[10] S. Brenner, L. Scott, The Mathematical Theory of Finite Element Methods, Texts in Applied Mathematics, third ed., vol. 15, Springer, 2007.
[11] P. Canham, The minimum energy of bending as a possible explanation of the biconcave shape of the red blood cell, J. Theor. Biol. 26 (1970) 61–81.
[12] T.A. Davis, Algorithm 832: UMFPACK, an unsymmetric-pattern multifrontal method, ACM Trans. Math. Software 30 (2004) 196–199.
[13] K. Deckelnick, G. Dziuk, C.M. Elliott, Computation of geometric partial differential equations and mean curvature flow, Acta Numer. 14 (2005) 139–232.
[14] A. Demlow, Higher-order finite element methods and pointwise error estimates for elliptic problems on surfaces, SIAM J. Numer. Anal. 47 (2009) 805–827.
[15] Q. Du, C. Liu, X. Wang, A phase field approach in the numerical study of the elastic bending energy for vesicle membranes, J. Comput. Phys. 198 (2004) 450–468.
[16] Q. Du, C. Liu, X. Wang, Simulating the deformation of vesicle membranes under elastic bending energy in three dimensions, J. Comput. Phys. 212 (2006) 757–777.
[17] G. Dziuk, Finite elements for the Beltrami operator on arbitrary surfaces, in: S. Hildebrandt, R. Leis (Eds.), Partial differential equations and calculus of variations, Lecture Notes in Mathematics, vol. 1357, Springer, 1988, pp. 142–155.
[18] G. Dziuk, Computational parametric Willmore flow, Numer. Math. 111 (2008) 55–80.
[19] G. Dziuk, C.M. Elliott, Finite elements on evolving surfaces, IMA J. Numer. Anal. 25 (2007) 385–407.
[20] G. Dziuk, C.M. Elliott, Surface finite elements for parabolic equations, J. Comput. Math. 25 (2007) 385–407.
[21] C. Eilks, C.M. Elliott, Numerical simulation of dealloying by surface dissolution via the evolving surface finite element method, J. Comput. Phys. 227 (2008) 9727–9741.
[22] C.M. Elliott, B. Stinner, A surface phase field model for two-phase biological membranes, submitted for publlication.
[23] E.A. Evans, Bending resistance and chemically induced moments in membrane bilayers, Biophys. J. 14 (1974) 923–931.
[24] F. Feng, W. Klug, Finite element modeling of liquid bilayer membranes, J. Comput. Phys. 220 (2006) 394–408.
[25] H. Garcke, B. Nestler, B. Stinner, F. Wendler, Allen–Cahn systems with volume constraints, Math. Model Methods Appl. Sci. 18 (2008) 1347–1381.
[26] M.E. Gurtin, Configurational forces as basic concepts of continuum physics, Applied Mathematical Sciences, vol. 137, Springer-Verlag, New York, 2000.
[27] C.-J. Heine, Computations of Form and Stability of Rotating Drops with Finite Elements, Ph.D. Thesis, Faculty for Mathematics, Informatics, and Natural Sciences, University of Aachen, 2003.
[28] C.-J. Heine, Isoparametric finite element approximation of curvature on hypersurfaces, J. Comput. Math., submitted for publication.
[29] W. Helfrich, Elastic properties of lipid bilayers: theory and possible experiments, Z. Naturforsch. C 28 (1973) 693–703.
[30] L. Hsu, R. Kusner, J. Sullivan, Minimizing the squared mean curvature integral for surfaces in space forms, Exp. Math. 1 (1992) 191–207.
[31] F. Jülicher, R. Lipowsky, Domain-induced budding of vesicles, Phys. Rev. Lett. 70 (1993) 2964–2967.
[32] F. Jülicher, R. Lipowsky, Shape transformations of vesicles with intramembrane domains, Phys. Rev. E 53 (1996) 2670–2683.
[33] L. Ma, W. Klug, Viscous regularization and *r*-adaptive remeshing for finite element analysis of lipid membrane mechanics, J. Comput. Phys. 227 (2008) 5816–5835.
[34] R. Rusu, An algorithm for the elastic flow of surfaces, Interface Free Boundaries 7 (2005) 229–239.
[35] A. Schmidt, K.G. Siebert, Design of adaptive finite element software: the finite element toolbox ALBERTA, Lecture Notes in Computational Science and Engineering, vol. 42, Springer, 2005.
[36] U. Seifert, Configurations of fluid membranes and vesicles, Adv. Phys. 46 (1997) 1–137.
[37] T. Taniguchi, Shape deformations and phase separation dynamics of two-component vesicles, Phys. Rev. Lett. 76 (1996) 4444–4447.
[38] U. Seifert, K. Berndl, R. Lipowsky, Shape transformations of vesicles-phase-diagram for spontaneous-curvature and bilayer-coupling models, Phys. Rev. A 44 (1991) 1182–1202.
[39] X. Wang, Q. Du, Modelling and simulations of multi-component lipid membranes and open membranes via diffuse interface approaches, J. Math. Biol. 56 (2008) 347–371.
[40] T.J. Willmore, Riemannian Geometry, Clarendon Press, Oxford, 1993.
[41] W. Wintz, H. Döbereiner, U. Seifert, Starfish vesicles, Europhys. Lett. 33 (1996) 403–408.

Please cite this article in press as: C.M. Elliott, B. Stinner, Modeling and computation of two phase geometric biomembranes using surface finite elements, J. Comput. Phys. (2010), doi:10.1016/j.jcp.2010.05.014